catalysts

MDPI

Review

Catalytic Steam Reforming of Methanol, Ethanol, and Glycerol for Hydrogen Production: A Critical Review of Reaction Chemistry, Catalyst Design, Performance Metrics, and Deactivation

Symbat Naurzkulova [1,*], Tolkyn Baizhumanova [2,3,*], Bakytgul Massalimova [4], Raushan Orazbekova [2,3] and Meruert Yerkibaeva [5]

[1] Department of Chemistry and Chemical Technology, Taraz University Named After M.Kh. Dulaty, Tole Bi Str. 60, Taraz 080000, Kazakhstan
[2] Laboratory of Oxidative Catalysis D.V. Sokolsky Institute of Fuel, Catalysis and Electrochemistry, 142 Kunaev Str., Almaty 050010, Kazakhstan; r.orazbekova@ifce.kz
[3] Department of Physical Chemistry, Catalysis and Petrochemistry Al-Farabi Kazakh National University, 71, al-Farabi Str., Almaty 050040, Kazakhstan
[4] Department of Chemistry and Chemical Technology, M. Kozybayev North Kazakhstan University, Pushkin Str. 80, Petropavlovsk 150000, Kazakhstan; bkmasalimova@ku.edu.kz
[5] Higher school of natural science, Pavlodar Pedagogical University Named After Alkey Margulan, Mira Str. 60, Pavlodar 140002, Kazakhstan; yerkibayeva_meruert@ppu.edu.kz
* Correspondence: naurzkulovasymbat@gmail.com (S.N.); tolkynbaizhumanova52@gmail.com (T.B.); Tel.: +7-707-193-75-22 (S.N.); +7-705-138-11-17 (T.B.)

Abstract

Catalytic steam reforming of oxygenated feedstocks is an important route to hydrogen-rich gases, but methanol, ethanol, and glycerol differ substantially in C–C bond content, reaction-network complexity, catalyst requirements, and deactivation behavior. This critical review compares the three feedstocks using feedstock-specific reaction chemistry rather than a generalized reforming mechanism. The stoichiometric maxima for complete conversion to CO_2 and H_2 are 3, 6, and 7 mol H_2 per mol of methanol, ethanol, and glycerol, respectively, but these limits are not treated as experimental catalyst rankings. Cu-based systems dominate low-temperature methanol steam reforming, whereas Ni-, Co-, bimetallic, noble-metal, and perovskite-derived catalysts are prominent in ethanol and glycerol reforming, where C–C activation and carbon suppression become increasingly important. Emphasis is placed on the nature and evolution of active sites, metal–support interactions, carbon deposition, sintering, regeneration, and the distinction among conversion, H_2 yield, H_2 selectivity, and dry-gas H_2 concentration. Recent studies through 2026 are integrated with foundational mechanistic work to identify catalyst-design principles and evidence gaps relevant to durable hydrogen production.

Keywords: hydrogen production; steam reforming; methanol; ethanol; glycerol; oxygenated feedstocks; catalyst design; catalyst deactivation; performance metrics; perovskite-derived catalysts

Check for updates

Academic Editor: Valeria La Parola

Received: 1 September 2026
Revised: 5 October 2026
Accepted: 9 October 2026
Published: 18 October 2026

Copyright: © 2026 by the authors. Licensee MDPI, Basel, Switzerland. This article is an open access article distributed under the terms and conditions of the Creative Commons Attribution (CC BY) license.

1. Introduction

Hydrogen is a central chemical feedstock and a potential low-carbon energy carrier when its production pathway limits greenhouse-gas emissions. Among thermochemical routes, catalytic steam reforming converts an oxygenated feedstock with water into an

H_2-rich gas while simultaneously coupling molecular activation, C–C/C–H bond transformation, water activation, and the water-gas shift reaction. The practical value of steam reforming therefore depends not only on equilibrium hydrogen production but also on catalyst activity, selectivity, heat demand, resistance to carbon deposition and sintering, and the origin of the feedstock and process energy. Methanol, ethanol, and glycerol are attractive comparative substrates because they are liquids that can be produced through different fossil, biomass-derived, or circular-carbon pathways and because their structures span progressively greater reaction complexity from a C_1 alcohol without a C–C bond to C_2 and C_3 oxygenates requiring C–C transformation [1–3].

This structural progression directly changes the chemistry imposed on the catalyst. Methanol (CH_3OH) contains one carbon atom and no C–C bond; its steam-reforming network is therefore dominated by methanol activation, oxygenated surface intermediates, CO-forming decomposition routes, and the water-gas shift (WGS) reaction [3–5]. Ethanol (C_2H_5OH) contains one C–C bond and can undergo dehydrogenation, dehydration, decomposition, reforming, and carbon-forming pathways; acetaldehyde and ethylene are important products or intermediates under relevant catalyst conditions [2,6,7]. Glycerol ($C_3H_8O_3$) contains two C–C bonds and three hydroxyl groups, producing a still broader network of oxygenated intermediates, C–C cleavage products, methane, CO, CO_2, and carbonaceous deposits [1,8–12].

The origin of the feedstock must be kept separate from the chemistry of the reforming reactor. Methanol may be produced from fossil-derived synthesis gas or from alternative carbon sources; ethanol may be obtained from biomass-derived sugars or lignocellulosic feedstocks; and glycerol is commonly generated as a co-product of biodiesel production [1–3]. Accordingly, the term "renewable hydrogen" should not be assigned solely based on the steam-reforming reaction. Any sustainability conclusion also depends on the upstream feedstock route, the energy used for steam generation and reactor heating, and the system boundary selected for environmental assessment.

Several conversion routes exist for oxygenated feedstocks, including steam reforming, partial oxidation, autothermal reforming, and CO_2-assisted reforming. These routes involve different co-reactants and cannot be represented by one universal stoichiometric equation for methanol, ethanol, and glycerol. To avoid the stoichiometric ambiguity that can arise from generalized expressions, the quantitative catalyst comparison in this review is restricted to steam reforming. Other reforming routes are mentioned only when needed for context and are not merged with the steam-reforming performance dataset.

Catalyst selection is feedstock dependent. Cu-based catalysts are widely studied for methanol steam reforming, whereas Ni-based catalysts are prominent in ethanol and glycerol steam reforming because they can promote C-C and C-H bond activation at elevated temperatures [2,3]. Co-containing, Ni-Co, noble-metal, and perovskite-derived systems are also considered in this review, but only within the feedstock and reaction conditions for which primary evidence is available. A catalyst composition or mechanistic interpretation demonstrated for ethanol is not assumed to provide the same behavior in glycerol reforming without a glycerol-specific primary source.

A second difficulty in cross-study comparison is the terminology used to report catalytic performance. Feedstock conversion, H_2 yield, H_2 selectivity, and H_2 concentration in the dry product gas describe different quantities and are not interchangeable. A high H_2 mole fraction in the dry gas does not, by itself, establish a high H_2 yield, and a high selectivity value does not establish high productivity when feed conversion is incomplete. This distinction is applied throughout the review, and each numerical value is retained on the calculation basis used by the primary source unless the information required for a rigorous recalculation is explicitly available.

Against this background, the objectives of the review are to: define feedstock-specific reaction networks for methanol, ethanol, and glycerol steam reforming; compare catalyst families using source-verified experimental data; keep conversion, H_2 yield, H_2 selectivity, and dry-gas H_2 concentration as separate performance descriptors; evaluate deactivation by carbon deposition, sintering, and related structural changes; and identify catalyst- and process-design conclusions that are supported directly by primary evidence rather than by transfer from another feedstock system.

2. Review Scope and Evidence-Handling Principles

The review is organized as a critical comparison of methanol, ethanol, and glycerol steam reforming. Quantitative catalyst values are retained using the terminology and calculation basis of the primary source, and conversion, H_2 yield, H_2 selectivity, and dry-gas H_2 concentration are treated as distinct descriptors (Table 1). Numerical values are not interconverted when the denominator or calculation basis cannot be established unambiguously.

Table 1. Performance descriptors used in the review and the rule applied to cross-study comparison.

Descriptor	Meaning in This Review	Comparison Rule
Feedstock conversion	Fraction or percentage of feedstock consumed.	Reported separately from product selectivity or yield.
H_2 yield	Hydrogen production on the basis explicitly defined by the original authors (e.g., mol H_2 per mol feed or % of a theoretical basis).	Not replaced by H_2 selectivity or gas composition.
H_2 selectivity	Source-defined selectivity toward H_2.	Retained only with the calculation basis stated or traceable in the primary paper.
Dry-gas H_2 concentration	Mole fraction or volume fraction of H_2 after removal of condensable water, when reported on a dry basis.	Treated as gas composition, not as H_2 yield.

Mechanistic conclusions are separated according to evidentiary strength: direct kinetic, product/intermediate, isotopic, in situ/operando, or post-reaction characterization is distinguished from interpretation by analogy. Full-text verification was used wherever accessible; when only an abstract or limited verified source text was available, that limitation is stated explicitly, and the corresponding value is not used for direct cross-study ranking. The detailed search strategy, source-verification procedure, and supplementary abbreviations are provided in Supplementary Note S1, while Supplementary Table S1 links quantitative entries to their source-defined metrics and reaction conditions.

Table 1 is used throughout the review to preserve the distinction among conversion, H_2 yield, H_2 selectivity, and dry-gas H_2 concentration.

3. Reforming Chemistry and Reaction Pathways

Methanol, ethanol, and glycerol can all be converted to hydrogen by steam reforming, but their reaction chemistry differs substantially. The equations below are overall stoichiometric reactions or experimentally reported reaction pathways; they should not be interpreted as one universal sequence of elementary surface steps. The relative contribution of each pathway depends on catalyst composition, active-site structure, support properties, temperature, steam-to-feed ratio, pressure, and residence time [3,4,8–12].

3.1. Methanol Steam Reforming

Methanol steam reforming (MSR) has the simplest overall carbon skeleton among the three systems because methanol contains no C-C bond. The net stoichiometric reaction for complete conversion to CO_2 and H_2 is

$$CH_3OH + H_2O \rightleftharpoons CO_2 + 3H_2 \quad (1)$$

Two additional reactions are central to interpretation of the product distribution:

$$CH_3OH \rightleftharpoons CO + 2H_2 \quad (2)$$

$$CO + H_2O \rightleftharpoons CO_2 + H_2 \quad (3)$$

Equation (2) is methanol decomposition and produces CO, whereas Equation (3) is the WGS reaction and consumes CO while generating additional H_2. Peppley et al. developed a reaction network for $Cu/ZnO/Al_2O_3$ in which steam reforming, methanol decomposition, and WGS are treated as distinct overall pathways, and their subsequent kinetic model retained the corresponding surface-reaction contributions [4,5]. Consequently, methanol conversion alone is insufficient for evaluating reformate quality; CO and CO_2 formation must also be considered.

Surface oxygenated species such as methoxy- and formate-related intermediates have been associated with MSR on different catalysts, but the dominant sequence is catalyst-dependent [3–5]. For this reason, Figure 1 is presented as a simplified reaction network rather than as a universal elementary mechanism.

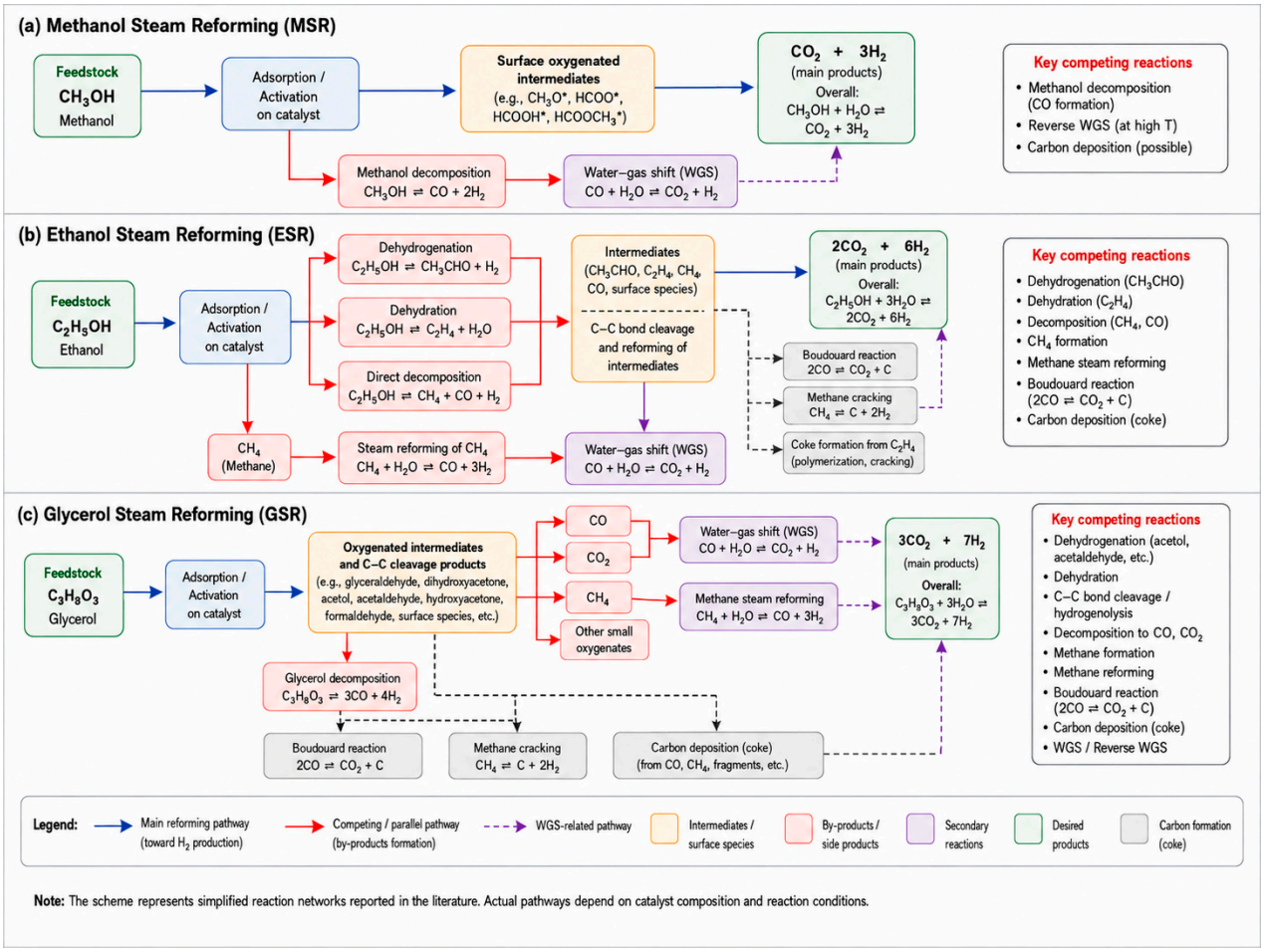

Figure 1. Simplified feedstock-specific reaction networks for methanol steam reforming (MSR), ethanol steam reforming (ESR), and glycerol steam reforming (GSR). The scheme distinguishes principal hydrogen-forming routes from selected competing, secondary, and carbon-forming pathways. It is a conceptual synthesis of reactions reported in the literature and should not be interpreted as a universal elementary mechanism; individual pathways depend on catalyst composition and reaction conditions. The asterisk (*) denotes an active site on the catalyst surface.

3.2. Ethanol Steam Reforming

Ethanol steam reforming (ESR) is more complex because complete conversion requires transformation of the C–C bond. The overall stoichiometric reaction is

$$C_2H_5OH + 3H_2O \rightleftharpoons 2CO_2 + 6H_2 \quad (4)$$

Important parallel or consecutive reactions reported for ESR include ethanol dehydrogenation, dehydration, and decomposition:

$$C_2H_5OH \rightleftharpoons CH_3CHO + H_2 \quad (5)$$

$$C_2H_5OH \rightleftharpoons C_2H_4 + H_2O \quad (6)$$

$$C_2H_5OH \rightleftharpoons CH_4 + CO + H_2 \quad (7)$$

Methane and CO formed in the reaction network can undergo further steam reforming and WGS:

$$CH_4 + H_2O \rightleftharpoons CO + 3H_2 \quad (8)$$

$$CO + H_2O \rightleftharpoons CO_2 + H_2 \quad (9)$$

Experimental work with a commercial $Ni/MgO/Al_2O_3$ catalyst used a reaction scheme in which acetaldehyde and ethylene appear as intermediates or side products and the final gas mixture contains H_2 together with carbon oxides and hydrocarbon products [6]. Independent microkinetic analysis on Rh(111) generated a large reaction network and showed that preferred routes to CO and CO_2 are selected from many possible elementary steps rather than from one universal sequence [7]. These studies support use of the terms "reaction network" and "competing pathways" in the present review.

The dehydration branch is particularly relevant to deactivation because C_2H_4 is an unsaturated carbon-containing species that can participate in subsequent polymerization, cracking, and carbon formation. In the revised scheme, coke formation from C_2H_4 is therefore represented as a carbon-forming pathway rather than by an unbalanced equation of the form "$C_2H_4 \rightarrow$ coke".

3.3. Glycerol Steam Reforming

Glycerol steam reforming (GSR) has the broadest reaction network of the three feedstocks because glycerol contains three carbon atoms, two C–C bonds, and three hydroxyl groups. The overall stoichiometric limit for complete conversion to CO_2 and H_2 is

$$C_3H_8O_3 + 3H_2O \rightleftharpoons 3CO_2 + 7H_2 \quad (10)$$

A useful overall decomposition pathway, together with WGS and methane steam reforming, can be written as

$$C_3H_8O_3 \rightleftharpoons 3CO + 4H_2 \quad (11)$$

$$CO + H_2O \rightleftharpoons CO_2 + H_2 \quad (12)$$

$$CH_4 + H_2O \rightleftharpoons CO + 3H_2 \quad (13)$$

The combination of Equation (11) with three equivalents of Equation (12) gives the overall stoichiometry in Equation (10), illustrating why seven moles of H_2 per mole of glycerol is a stoichiometric maximum rather than an experimentally guaranteed yield.

Primary GSR studies report H_2 together with CO_2, CO, and CH_4, confirming the coexistence of reforming, WGS, methane formation, and secondary reactions [8–12]. Experiments over $Co\text{-}Ni/Al_2O_3$, Ni/Al_2O_3, and supported Rh or Ni catalysts also show

that catalyst stability is strongly affected by carbon deposition and by the distribution of intermediate products. Glycerol-derived oxygenates may undergo dehydration, dehydrogenation, hydrogenolysis, condensation, and C-C cleavage before their carbon is fully converted to gaseous products; the relative contribution of these routes is catalyst- and condition-dependent [9–12].

Two selected carbon-forming reactions that are relevant to GSR are

$$2CO \rightleftharpoons CO_2 + C \quad (14)$$

$$CH_4 \rightleftharpoons C + 2H_2 \quad (15)$$

Equations (14) and (15) represent the Boudouard reaction and methane decomposition, respectively. They are included as selected carbon-forming routes rather than as an exhaustive description of coke formation. Carbon can also arise from cracking, condensation, and polymerization of larger intermediates; the dominant route depends on catalyst surface chemistry and operating conditions [9,11,12].

3.4. Comparative Reaction Chemistry

The principal chemical differences and competing pathways are summarized in Table 2.

Table 2. Comparative chemical characteristics of methanol, ethanol, and glycerol steam reforming.

Feature	MSR	ESR	GSR
Feedstock	CH_3OH	C_2H_5OH	$C_3H_8O_3$
Carbon atoms	1	2	3
C–C bonds	0	1	2
Theoretical H_2 maximum (mol H_2/mol feed)	3	6	7
Principal chemistry challenge	CO control and product distribution	C-C cleavage; dehydration and carbon suppression	Complex C_3 network; methane and carbon suppression
Selected competing pathways	Methanol decomposition; WGS/reverse WGS	Dehydrogenation; dehydration; decomposition; CH_4 reforming	Decomposition; WGS; CH_4 formation/reforming; carbon formation

The three feedstocks show a stepwise increase in reaction-network complexity from C_1 to C_3. Methanol requires no C-C bond cleavage, ethanol requires transformation of one C-C bond, and glycerol contains two C-C bonds together with three hydroxyl groups. The stoichiometric H_2 maxima follow directly from the balanced overall steam-reforming equations and must not be confused with experimental yield or selectivity.

The values 3, 6, and 7 mol H_2 per mol feed are stoichiometric maxima for complete conversion to CO_2 and H_2. They are not experimental catalyst-performance values and should not be used to rank catalysts without accounting for the metric definition, feed conversion, product distribution, and reaction conditions.

3.5. Implications for Catalyst Comparison

The reaction chemistry establishes the basis for a feedstock-specific catalyst comparison. For MSR, catalyst evaluation must include methanol activation together with control of CO formation. For ESR, C-C activation must be balanced against dehydration, methane formation, and carbon-producing pathways. For GSR, the broader C_3 network requires simultaneous control of oxygenated intermediates, C–C cleavage, methane formation/reforming, WGS, and carbon deposition.

These differences are also a methodological constraint on the review. Evidence for a Ni-Co, perovskite-derived, or other catalyst in ESR cannot be transferred automatically to GSR, and evidence obtained in GSR cannot be assumed to describe MSR. Subsequent catalyst sections should therefore report each material within the exact feedstock–catalyst–operating-condition combination of the primary study and should distinguish experimentally demonstrated behavior from mechanistic interpretation.

4. Thermodynamic Framework and Operating Variables of Steam Reforming

Section 3 established feedstock-specific reaction networks for methanol, ethanol, and glycerol. The purpose of the present section is therefore not to introduce another generalized mechanism but to define the thermodynamic constraints used to interpret the catalyst data discussed later in the review. Thermodynamic equilibrium calculations identify product distributions that are accessible under a specified set of temperature, pressure, feed composition, and admissible chemical species. Catalytic experiments, in contrast, determine whether those states are approached at an experimentally relevant rate and whether kinetic side pathways or catalyst deactivation prevent the equilibrium state from being reached. Thermodynamic predictions and catalytic performance are consequently treated as complementary, but not interchangeable, forms of evidence [13–19].

4.1. Equilibrium Basis and Limits of Thermodynamic Comparison

Thermodynamic analyses of alcohol steam reforming commonly employ direct minimization of the total Gibbs free energy subject to elemental-balance constraints, although stoichiometric equilibrium formulations have also been used. The calculated result is conditional on the species set included in the minimization, the thermodynamic model used for the gas phase, the representation of condensed carbon, and the chosen feed composition. These modeling choices are not secondary details. For methanol, Faungnawakij et al. explicitly examined the effect of the admissible product species and included graphite together with gaseous hydrocarbons and oxygenates in the equilibrium calculation [13]. For ethanol, Lima da Silva et al. showed that stable and metastable product sets can give markedly different carbon activities [16], while Díaz Alvarado and Gracia demonstrated that the assumed solid-carbon representation itself changes predicted carbon-deposition behavior [19].

Accordingly, terms such as “optimum temperature”, “carbon-free region”, or “maximum hydrogen production” are used in this review only within the modeling domain of the cited primary study. They are not transferred directly from one feedstock to another and are not treated as universal operating windows. The balanced overall steam-reforming equations given in Section 3 provide stoichiometric limits, whereas the equilibrium studies summarized below define how temperature, pressure, and steam addition redistribute products within specific thermodynamic models.

4.2. Temperature and Pressure Effects: Feedstock-Specific Evidence

For methanol steam reforming, Faungnawakij et al. minimized the Gibbs free energy over 25–1000 °C, 0.5–3 atm, and steam-to-carbon ratios (S/C) from 0 to 10 [13]. Within their restricted product basis containing CH_3OH, H_2O, H_2, CO, and CO_2, complete equilibrium conversion of methanol was obtained at S/C = 1 above 200 °C at atmospheric pressure. When a broader species set including methane, graphite, hydrocarbons, higher alcohols, and dimethyl ether was considered, the predicted equilibrium boundaries depended on both temperature and S/C. The same study found that the temperature required to enter a coke-free equilibrium region decreased as S/C increased, whereas pressure in the investigated

0.5–3 atm range had little influence on complete methanol conversion [13]. These results are therefore evidence for the sensitivity of MSR equilibrium to species selection and steam addition, not a universal prescription that every MSR catalyst will achieve equilibrium above a single threshold temperature.

For ethanol steam reforming, García and Laborde examined equilibrium over 400–800 K, 1–9 atm, and water-to-ethanol feed ratios from 0:1 to 10:1 using a non-stoichiometric formulation [14]. Their calculations identified temperatures above 650 K, atmospheric pressure, and excess water as conditions favorable to hydrogen production, with methane minimized and carbon formation thermodynamically inhibited within the model. Vasudeva et al. subsequently re-examined ESR thermodynamics under carbon-forming conditions and extended the calculations to higher water-to-ethanol ratios and temperatures relevant to dilute ethanol feeds [15]. The key implication for this review is not a single optimum temperature, but the consistent thermodynamic tendency for ESR to require more severe conditions than MSR because the C-C bond must be transformed and methane- and carbon-forming states must be suppressed.

For glycerol steam reforming, Adhikari et al. performed direct Gibbs free-energy minimization over 600–1000 K, 1–5 atm, and water-to-glycerol molar feed ratios from 1:1 to 9:1 [17]. In their equilibrium model, the most favorable conditions for hydrogen production occurred above 900 K at atmospheric pressure and at a water-to-glycerol ratio of 9:1; under those conditions methane was minimized, and carbon formation was thermodynamically inhibited. These values must be interpreted with their original feed-ratio definition: a water-to-glycerol ratio of 9 corresponds to S/C = 3 for pure glycerol because each glycerol molecule contains three carbon atoms. Rossi et al. independently applied Gibbs-energy minimization to ethanol and glycerine systems and compared their calculations with literature conditions, further illustrating that feedstock identity and operating variables must be evaluated together rather than through a common temperature rule [18]. The primary thermodynamic studies and the operating-variable domains used for the comparative analysis are summarized in Table 3.

Table 3. Primary thermodynamic studies used to define the operating-variable discussion in Section 4.

Primary Study	Domain Examined	Directly Supported Use in This Review
MSR: Faungnawakij et al. [13]	Gibbs minimization; 25–1000 °C; 0.5–3 atm; S/C = 0–10; multiple product-species sets including graphite.	Shows that MSR equilibrium and the predicted coke-free boundary depend on S/C and on the species admitted to the model; complete conversion in a restricted basis was predicted at S/C = 1 above 200 °C and 1 atm.
ESR: García and Laborde [14]	Non-stoichiometric equilibrium; 400–800 K; 1–9 atm; H_2O/EtOH = 0–10.	Supports the thermodynamic benefit of higher temperature, atmospheric pressure, and excess water for H_2 production within the investigated ESR domain.
ESR: Lima da Silva et al. [16]	Gibbs minimization; stable and metastable systems; carbon activity evaluated for low- and high-contact-time representations.	Demonstrates that carbon-deposition predictions depend strongly on the assumed intermediate/product set and therefore cannot be equated directly with real catalyst coking.
GSR: Adhikari et al. [17]	Direct Gibbs minimization; 600–1000 K; 1–5 atm; H_2O/glycerol = 1–9.	Supports high-temperature, low-pressure, steam-rich equilibrium conditions for H_2 production; H_2O/glycerol = 9 is S/C = 3 for pure glycerol.
ESR/GSR: Rossi et al. [18]	Gibbs-energy minimization applied to ethanol and glycerine under literature-relevant temperature and pressure conditions.	Supports feedstock-specific equilibrium comparison and cautions against interpreting thermodynamic predictions independently of the study's definitions and conditions.
ESR carbon: Díaz Alvarado and Gracia [19]	Thermodynamic ESR analysis with different representations of deposited carbon.	Supports the conclusion that the predicted carbon boundary depends on the thermodynamic representation of the condensed carbon phase.

4.3. Steam-to-Feed Ratio Versus Steam-to-Carbon Ratio

A major source of inconsistency in the reforming literature is the interchangeable use of water-to-feed ratio and steam-to-carbon ratio. They are not the same quantity for multi-carbon feedstocks. To remove this ambiguity, the present review defines the carbon-normalized steam-to-carbon ratio as

$$S/C = n(H_2O,in)/[N_C \cdot n(feed,in)] \quad (16)$$

where N_C is the number of carbon atoms in one molecule of the oxygenated feedstock. Thus, for pure methanol (N_C = 1), H_2O/CH_3OH and S/C have the same numerical value. For ethanol (N_C = 2), H_2O/C_2H_5OH = 2(S/C), and for glycerol (N_C = 3), $H_2O/C_3H_8O_3$ = 3(S/C). For example, the H_2O/glycerol ratio of 9:1 examined by Adhikari et al. [17] corresponds to S/C = 3, not S/C = 9.

In the quantitative catalyst tables of this review, the feed ratio will therefore be reported using the terminology of the original source, with a separate carbon-normalized S/C value added only when the feed composition makes the conversion unambiguous. This rule is important because direct comparison of "S/C = 3" in an ethanol paper with "H_2O/glycerol = 3" in a glycerol paper would otherwise compare two different steam dosages. Thermodynamically, increasing steam generally enlarges the equilibrium region in which methane and condensed carbon are suppressed [13–17]; however, excessive steam also increases the process duty associated with vaporization and heating. The latter is a process-level trade-off and should not be confused with an intrinsic catalyst property.

4.4. Carbon Formation: Equilibrium Prediction Versus Catalytic Reality

Carbon deposition requires particular caution because a thermodynamic carbon-free region does not guarantee coke-free catalyst operation, and a predicted carbon-favorable state does not quantify the actual rate or morphology of coke formation. The discrepancy arises because reforming catalysts can generate short-lived oxygenates, olefins, surface fragments, and metal-bound carbon species that are not necessarily represented in a conventional equilibrium species set. Equilibrium calculations therefore define thermodynamic driving forces, whereas the observed amount and type of coke are controlled additionally by reaction kinetics, catalyst acid-base properties, metal ensemble size, oxygen transfer, residence time, and the ability of steam to remove surface carbon.

This distinction is demonstrated explicitly for ESR by Lima da Silva et al. [16]. When the thermodynamic system was constructed to represent very low contact times and was dominated by ethylene and acetaldehyde, the calculated carbon activity remained far above unity over the investigated temperature range and was only weakly affected by the inlet steam-to-ethanol ratio. In a more stable product system representing longer contact times, carbon activity was much lower and became strongly dependent on steam addition. Díaz Alvarado and Gracia further showed that changing the representation of deposited carbon changes the predicted thermodynamic carbon boundary [19]. These results justify two rules adopted in the present review: equilibrium carbon maps are not used as direct measurements of catalyst coking resistance, and claims of coke suppression are accepted only when supported by experimental evidence such as carbon analysis, thermogravimetric oxidation, microscopy, spectroscopy, or stable time-on-stream data.

4.5. Thermodynamic Limits and Experimental Performance Metrics

The stoichiometric maxima derived from the balanced overall reactions in Section 3 are 3 mol H_2 per mol CH_3OH, 6 mol H_2 per mol C_2H_5OH, and 7 mol H_2 per mol $C_3H_8O_3$. These values are reference limits for complete conversion to CO_2 and H_2 and are not experimental catalyst yields. A thermodynamic model may also report an equilibrium

H_2 mole fraction, an equilibrium number of moles of H_2, or a yield normalized to a theoretical maximum; those quantities must not be relabeled as experimental H_2 selectivity or dry-gas concentration.

For this reason, the performance-metric policy introduced in Section 2 is maintained throughout the catalyst sections. Conversion, H_2 yield, H_2 selectivity, and dry-gas H_2 concentration are retained in separate columns and on the basis defined by each primary source. No numerical value is converted from selectivity to yield, or from dry-gas composition to yield, unless the original paper supplies all information required for an exact calculation. Thermodynamic values are identified explicitly as equilibrium calculations and are not placed in the same ranking column as experimentally measured catalyst performance. This separation directly prevents a high dry-gas H_2 fraction from being interpreted as a high feed-based hydrogen yield.

4.6. Implications of Thermodynamic Constraints for Catalyst Evaluation

The thermodynamic analysis outlined above provides a framework for interpreting catalytic performance, but it does not constitute a direct measure of catalyst activity or durability. Temperature, pressure, steam-to-feed ratio, and feedstock composition determine the thermodynamically accessible product distribution, whereas the extent to which equilibrium is approached depends on catalyst composition, active-site structure, reaction kinetics, mass-transfer limitations, and deactivation phenomena. Consequently, catalyst performance should be evaluated within the specific thermodynamic and experimental domain in which the measurements were obtained.

This consideration is particularly important when comparing methanol, ethanol, and glycerol steam reforming. Methanol reforming can achieve high equilibrium conversion at substantially lower temperatures than ethanol or glycerol reforming, whereas the latter two systems require more severe conditions to promote C-C bond transformation and suppress methane- and carbon-forming pathways. Thus, a catalyst operating efficiently at a comparatively low temperature in MSR cannot be ranked directly against an ESR or GSR catalyst tested at higher temperature without accounting for the different thermodynamic requirements of the feedstocks.

Steam addition must likewise be interpreted using an unambiguous basis. Water-to-feed ratio and carbon-normalized steam-to-carbon ratio are numerically identical only for methanol and differ for ethanol and glycerol. Comparisons based solely on the reported numerical value of the steam ratio can therefore be misleading unless the original definition is retained.

Finally, equilibrium predictions of carbon formation should be regarded as indicators of thermodynamic driving force rather than direct evidence of catalyst resistance to coking. Experimental assessment of catalyst durability requires time-on-stream testing together with appropriate post-reaction characterization, including carbon quantification, thermogravimetric or temperature-programmed oxidation analysis, microscopy, spectroscopy, or measurements of metal sintering. Accordingly, the catalyst comparisons presented in this review are interpreted using both the operating conditions and the specific performance metrics reported in the primary studies.

5. Methanol Steam Reforming: Catalyst Systems and Source-Verified Performance

Methanol steam reforming (MSR) is catalytically distinct from ethanol and glycerol steam reforming because methanol contains no C-C bond and can be converted at substantially lower temperatures. For catalyst comparison, the central performance questions are therefore not C-C bond cleavage but (i) the rate of methanol activation, (ii) selectivity between the CO_2-forming reforming route and CO-forming pathways, and (iii) maintenance

of the active surface against thermal or chemical deactivation. The reaction network and thermodynamic constraints were defined in Sections 3 and 4; the present section focuses only on catalyst evidence that can be traced to primary experimental studies [20–28].

Cu-containing catalysts dominate the verified MSR literature used here, but the term 'Cu-based catalyst' does not identify a single universal active phase. Activity and selectivity vary with Cu dispersion, reduction state, metal-support interfacial structure, preparation history, and the chemical properties of the support or promoter. Accordingly, mechanistic interpretations reported for Cu/Zn/Al, Cu/CeO_2, or Cu/ZrO_2 are not assumed to be interchangeable. Quantitative values are retained using the terminology of the original publication and are not reclassified as H_2 yield, H_2 selectivity, or dry-gas concentration unless the source explicitly defines them as such.

Active-site identity in MSR is dynamic rather than fixed. Cu^0 and Cu^+ populations, Cu–oxide interfacial sites, oxygen vacancies, particle size, and support phase can change during reduction and reaction. Recent operando and in situ studies show that water activation and formate chemistry depend on the evolving Cu oxidation-state distribution and on $Cu–ZrO_2$ or $Cu–CeO_2$ interfacial environments [28–33]. Accordingly, catalyst state should be described both before reaction and under/after steam-reforming conditions; a nominal precursor composition alone is insufficient to define the catalytically relevant surface.

5.1. Cu/Zn/Al Systems: Preparation Method and Reducibility

The importance of preparation history was demonstrated directly by Shen and Song, who compared impregnation, co-precipitation, and hydrothermal synthesis for Cu/Zn/Al catalysts [21]. At 230 °C, the best co-precipitated catalyst gave 99–100% methanol conversion, while the paper reported 71–76% 'H_2 production' and a CO concentration of 0.05–0.15% at H_2O/CH_3OH = 1.43. The accessible source text does not establish a sufficiently explicit denominator for the 71–76% 'H_2 production' value. It is therefore retained only as the authors' original terminology and is not interpreted as H_2 yield, H_2 selectivity, or dry-gas H_2 concentration and is not used for direct cross-study comparison.

The importance of preparation history was demonstrated directly by Shen and Song, who compared impregnation, co-precipitation, and hydrothermal synthesis for Cu/Zn/Al catalysts [21]. At 230 °C, the best co-precipitated catalyst gave 99–100% methanol conversion, while the paper reported H_2 production of 71–76% and a CO concentration of 0.05–0.15% at H_2O/CH_3OH = 1.43. Importantly, the authors related better low-temperature activity to a lower Cu-reduction temperature. In Table 4, 'H_2 production' is retained exactly as the terminology used by that source; it is not relabeled as H_2 yield or H_2 selectivity because the calculation basis is not assumed to be equivalent.

Table 4. Representative MSR catalyst data verified against primary publications. Performance descriptors are retained using the source's own terminology and should not be directly ranked across rows without accounting for metric definition and operating conditions.

Catalyst/Formulation	Key Conditions	Methanol Conversion	H_2 Metric as Reported	CO Metric as Reported	Stability/Deactivation Evidence	Ref.
Cu/Zn/Al; best co-precipitated sample	230 °C; H_2O/CH_3OH = 1.43	99–100%	H_2 production: 71–76% (source terminology; denominator not verified in accessible source text; not used for direct cross-study comparison)	CO concentration: 0.05–0.15%	Preparation method controlled reducibility and low-temperature activity.	[21]
CuO/CeO_2	260–300 °C; continuous/discontinuous operation	Initial conversion >80%	H_2 reported as a main product; source also reports SH_2 = 100%	CO selectivity: 3.8% at 260 °C to 6.4% at 300 °C after ~370 min	Conversion decreased with TOS; air treatment at 400 °C restored much of the initial activity.	[22]

Table 4. *Cont.*

Catalyst/Formulation	Key Conditions	Methanol Conversion	H_2 Metric as Reported	CO Metric as Reported	Stability/Deactivation Evidence	Ref.
$CuO/CeO_2/ZrO_2$; best ratio 8:1:1 (wt.)	MSR; 5 h stability comparison	n.r. in abstract	n.r. in abstract	n.r. in abstract	No deactivation reported for CuO/ZrO_2 and $CuO/CeO_2/ZrO_2$ during the 5 h test; CuO/CeO_2 deactivated.	[23]
Cu-MCM-41	250 °C; CH_3OH/H_2O = 1:3; separate TOS at 300 °C	~74% during stable 10–40 h interval at 300 °C	H_2 selectivity: 100% at 250 °C (source terminology)	~6% CO at 250 °C	40 h TOS at 300 °C; no apparent deactivation from 10 to 40 h.	[24]
ZrO_2-promoted CeO_2-Cu/KIT-6 (THF-prepared)	300 °C	96%	H_2 selectivity: 99.8%	CO selectivity: 0.7%	Stability evaluated over 100 h; duration reported without assuming zero deactivation.	[25]
Cu/Y1.5Ce0.84 Ru0.04O4; microchannel coating	Performance at 250 °C; spent catalyst after 32 h at 300 °C	99.5% at 250 °C	H_2 selectivity: 98.7% at 250 °C	CO selectivity: 1.4% at 250 °C	No detectable coke after 32 h at 300 °C by FE-SEM and TGA.	[26]
Ga-doped Cu/Al_2O_3 aerogel; optimized composition	260 °C	100%	n.r. in abstract	No CO formation reported	Primary study used Ga promotion to suppress CO; quantitative long-term stability not used here.	[27]

Abbreviations: TOS, time-on-stream; n.r., not reported in the abstract or directly verified source text used for this audit. The table deliberately retains expressions such as 'H_2 production', 'H_2 selectivity', 'CO concentration', and 'CO selectivity' exactly as stated by the corresponding primary publication. These quantities are not treated as interchangeable.

5.2. Reducible Oxide Supports: CeO_2 and ZrO_2

Ceria-supported Cu illustrates why activity and stability must be evaluated separately. Tonelli et al. studied a CuO/CeO_2 catalyst under continuous and discontinuous operation between 260 and 300 °C [22]. The fresh catalyst showed initial methanol conversions above 80%, with H_2 and CO_2 as the main products. The source reported CO selectivity increasing from 3.8% at 260 °C to 6.4% at 300 °C after approximately 370 min on stream, while conversion decreased with time. Air treatment at 400 °C restored much of the initial activity, demonstrating that the observed deactivation was at least partly reversible. This study is therefore used here primarily as evidence that high initial activity does not by itself establish long-term catalyst stability.

ZrO_2-containing systems provide a complementary example. Oguchi et al. reported that, within their CuO/CeO_2-based series, the optimum CuO content in CuO/CeO_2 was 80 wt.% and the best $CuO/CeO_2/ZrO_2$ weight ratio was 8:1:1 [23]. The CuO/CeO_2 material gradually lost activity, whereas CuO/ZrO_2 and $CuO/CeO_2/ZrO_2$ showed no detectable deactivation during the 5 h test reported in that study. Their XRD, TPR, and XANES results also showed that the copper state under reaction conditions depended strongly on the oxide environment. The result supports a support-dependent Cu chemistry rather than a universal assignment of one Cu oxidation state as the active phase.

More recent in situ and operando work by Ploner et al. further demonstrated that the MSR behavior of Cu/ZrO_2 depends on the ZrO_2 polymorph, synthesis route, precursor, and resulting surface properties [28]. Their comparative study focused specifically on how these variables alter CO_2 selectivity at the Cu-ZrO_2 interface. For the present review, this work is used as mechanistic evidence that the support surface participates in determining selectivity; it is not used to assign a single universal Cu-ZrO_2 elementary pathway to all zirconia-supported catalysts.

5.3. Mesoporous, Composite, and Microstructured Cu Catalysts

Support architecture can modify both dispersion and time-on-stream behavior. Abrokwah et al. synthesized a series of M-MCM-41 catalysts (M = Cu, Co, Ni, Pd, Zn, and Sn) under comparable preparation and test conditions [24]. Cu-MCM-41 gave the highest activity within that series. At 250 °C and a methanol/water molar ratio of 1:3, the paper reported 100% H_2 selectivity, approximately 6% CO, and no methane formation. In a separate 40 h time-on-stream test at 300 °C, Cu-MCM-41 maintained approximately 74% methanol conversion with no apparent deactivation between 10 and 40 h. Because the H_2 and CO descriptors use the source's own definitions, they are preserved as source-reported metrics and are not arithmetically combined.

Taghizadeh and Hosseini Abbandanak investigated CeO_2-Cu/KIT-6 catalysts prepared with different impregnation media and evaluated ZrO_2 promotion [25]. The ZrO_2-promoted CeO_2-Cu/KIT-6 catalyst prepared using tetrahydrofuran gave 96% methanol conversion, 99.8% source-reported H_2 selectivity, and 0.7% source-reported CO selectivity at 300 °C. The authors attributed the improved performance to smaller Cu particles and improved dispersion and evaluated catalytic stability over 100 h. The present review reports the 100 h value as the duration of the stability test; it does not convert that duration into a claim of zero deactivation unless the full time-on-stream profile supports such a statement.

Khani et al. deposited Cu on a $Y_{1.5}Ce_{0.84}Ru_{0.04}O_4$ support in a microchannel plate reactor [26]. At 250 °C, the source reported 99.5% methanol conversion, 98.7% H_2 selectivity, and 1.4% CO selectivity. A spent-catalyst examination after 32 h on stream at 300 °C showed no detectable coke by FE-SEM and thermogravimetric analysis. The performance values at 250 °C and the coke-resistance observation at 300 °C are kept as separate experimental conditions in Table 4 and are not merged into a single operating point.

Promoter chemistry can also strongly affect CO formation. In a 2023 primary study, Zhou et al. investigated Ga-doped Cu/Al_2O_3 aerogels and reported complete methanol conversion without detectable CO formation at 260 °C for the optimized material [27]. The significance of this result is the experimentally demonstrated suppression of CO under the authors' stated conditions; it should not be generalized to all Ga-containing Cu catalysts or to other space velocities and feed compositions without direct comparison. The representative MSR catalyst performance and stability data discussed above are summarized in Table 4.

5.4. Deactivation and Stability: What Is Actually Demonstrated

The verified MSR literature shows that deactivation cannot be reduced to a single mechanism. In CuO/CeO_2, Tonelli et al. observed pronounced loss of conversion with time on stream and substantial activity recovery after oxidative regeneration, indicating a reversible component to deactivation under their conditions [22]. Oguchi et al. found a clear support effect: CuO/CeO_2 lost activity, while ZrO_2-containing Cu catalysts did not show measurable deactivation during a shorter 5 h experiment [23]. In Cu-MCM-41, by contrast, a stable conversion plateau was reported from 10 to 40 h at 300 °C [24]. Khani et al. supplied direct post-reaction evidence for the absence of detectable coke after 32 h at 300 °C on their microchannel catalyst [26]. These studies therefore support catalyst-specific stability claims, but they do not justify a universal statement that CeO_2, ZrO_2, mesoporous silica, or any particular promoter always prevents deactivation.

This distinction is important when comparing stability claims. 'Stable for 5 h', 'tested for 100 h', 'no apparent deactivation between 10 and 40 h', and 'no detectable coke after 32 h' are four different experimental statements. They are therefore kept separate in this review. A stability duration is not interpreted as evidence of zero deactivation unless the

activity profile demonstrates that behavior, and absence of coke does not by itself exclude other loss mechanisms such as Cu sintering, surface reconstruction, or reversible poisoning.

5.5. Evidence-Based Design Implications for MSR

Taken together, the source-verified studies support several conclusions for MSR catalyst design. First, Cu dispersion and reducibility are strongly affected by preparation method, as shown for Cu/Zn/Al [20,21]. Second, oxide supports are chemically active components of the catalyst environment rather than inert carriers: CeO_2 and ZrO_2 alter Cu stability, reduction behavior, and product selectivity [22,23,28]. Third, mesoporous and microstructured supports can produce high conversion and favorable source-reported H_2/CO metrics, but their performance must be interpreted together with reactor configuration and time-on-stream evidence [24–26]. Fourth, promoter effects can be highly specific; the Ga-doped Cu/Al_2O_3 result demonstrates CO suppression for a particular catalyst and condition rather than a general rule for all Ga-containing formulations [27].

The verified evidence does not support ranking all MSR catalysts by a single percentage value. The 99–100% methanol conversion reported for a co-precipitated Cu/Zn/Al catalyst at 230 °C [21], the 99.8% source-reported H_2 selectivity for ZrO_2-promoted CeO_2-Cu/KIT-6 at 300 °C [25], and the 99.5% conversion/98.7% H_2 selectivity reported for a microchannel $Cu/Y_{1.5}Ce_{0.84}Ru_{0.04}O_4$ system at 250 °C [26] describe different catalysts, reactors, and metrics. Accordingly, subsequent cross-feedstock comparisons will use these values as source-specific performance descriptors, not as evidence for a universal 'best catalyst'.

Recent primary studies strengthen the support- and interface-dependent interpretation of Cu-based MSR. Zhang et al. [29] prepared Zr-modified Cu/ZnO catalysts and found that a Zn/Zr molar ratio of 5 generated a high population of Cu-ZnO/Cu-$ZnZrO_x$ interfacial sites and the highest source-reported H_2 production rate, 117.4 mmol H_2 $gcat^{-1}$ h^{-1} at 200 °C. Song et al. [30] independently showed that a mixed-phase Cu/ZrO_2-Al_2O_3 catalyst containing 81.4% monoclinic ZrO_2 reached 88.5% methanol conversion and an H_2 production rate of 104.6 μmol $gcat^{-1}$ s^{-1} at 275 °C; a 9 h stability experiment was also reported. These values are retained on their original bases and are not converted into H_2 yield or selectivity.

Recent mechanistic work also clarifies why a single static Cu oxidation state should not be assigned as universally active. Ma et al. [31] used $Cu/Ce_{1-x}Zr_xO_2$ catalysts together with experiments and DFT calculations to show complementary functions of Cu^+ and Cu^0, with Cu^+ sites mainly associated with CH_3OH adsorption/activation and Cu^0 sites with H_2O activation and the WGS pathway; the best-performing composition had a surface Cu^+/Cu^0 ratio close to unity. Liu et al. [32] subsequently showed on Cu/Al_2O_3 that water activation dynamically oxidizes Cu^0 to Cu^+-OH species and identified formate dehydrogenation as a low-temperature rate-determining step. In 2026, Liu et al. [33] directly linked enhanced MSR to a dynamic electronic metal-support interaction at ZnO_x/Cu interfaces, where bidirectional electron transfer facilitates water activation and Cu^+/Cu^0 redox cycling. These findings reinforce dynamic, catalyst-specific interfacial descriptions rather than a universal single-site model.

6. Ethanol Steam Reforming: Catalyst Systems and Source-Verified Performance

Ethanol steam reforming (ESR) imposes catalyst requirements that are substantially different from those of methanol steam reforming because the reaction network includes C-C bond transformation together with dehydrogenation, dehydration, methane-forming, water–gas-shift, and carbon-forming pathways. The balanced overall reaction and the principal competing pathways were defined in Section 3, while the thermodynamic effects

of temperature, pressure, and steam addition were considered in Section 4. The present section therefore focuses on experimentally demonstrated catalyst behavior. Quantitative values are retained using the terminology and calculation basis of the primary source; H_2 yield, H_2 selectivity, and gas-phase H_2 concentration are not treated as interchangeable quantities [2,34–40].

For ESR, high ethanol conversion alone is an insufficient performance criterion. A useful catalyst must also promote conversion of oxygenated intermediates and C-C cleavage while limiting ethylene formation, methane accumulation, carbon deposition, and metal sintering. The relative importance of these functions varies with active metal, support chemistry, steam dosage, temperature, space velocity, and time-on-stream. Accordingly, the discussion below is organized around source-verified catalyst functions rather than around a universal ranking.

For ESR, the catalytically relevant working state is determined by reduction and reaction-induced restructuring rather than by nominal precursor composition alone. Reduced Ni^0 or Co^0 ensembles promote C–C and C–H activation, whereas alloying, metal–support interaction, support acid–base properties, oxygen-transfer capacity, and carbon coverage modify the balance among dehydrogenation, dehydration, reforming, and coke formation. The studies summarized in this section document changes in metal dispersion, oxidation state, alloy character, support interaction, and spent-catalyst carbon before and after catalysis [34–45]; these descriptors are therefore considered together with conversion and H_2 metrics.

6.1. Ni- and Co-Based Catalysts: Active Metal and Support Effects

Ni and Co are among the most widely investigated non-noble active metals for ESR, but their behavior depends strongly on the support and on the reaction pathway favored under the selected conditions. Freni et al. compared MgO-supported Ni and Co under simulated molten-carbonate fuel-cell conditions [34]. Ni/MgO showed higher activity and higher source-reported H_2 selectivity than Co/MgO; the authors related this difference to the lower tendency of Ni to undergo oxidation during reaction and to promote CO methanation and ethanol-decomposition pathways. Importantly, the basic MgO support strongly depressed coke formation. An endurance test at a gas hourly space velocity of 10,000 h^{-1} was continued for 630 h, providing unusually long time-on-stream evidence for this catalyst family [34]. This result supports the beneficial role of a basic carrier under those conditions, but does not imply that MgO universally eliminates carbon formation for all Ni- or Co-based formulations.

Bichon et al. examined approximately 12% Co supported on Al_2O_3, SiO_2, and TiO_2 and included a commercial Ni/Al_2O_3 catalyst as a benchmark at atmospheric pressure [35]. Selectivity depended strongly on the support, particularly at low and intermediate temperatures. Acetaldehyde was important at lower temperature, whereas CO, CO_2, and CH_4 dominated at higher temperature; ethylene formation was especially evident on alumina-supported materials. Above 550 °C, ethanol conversion was complete, and the H_2 yield approached 5 mol H_2 per mol ethanol converted. The authors nevertheless reported high carbon formation for the alumina-supported Co and Ni catalysts despite acceptable deactivation rates [35]. This study illustrates why high conversion and high H_2 production must be considered together with direct carbon-deposition evidence.

A direct comparison on zirconia was reported by Padilla et al. for lanthana-promoted Ni/ZrO_2 and Co/ZrO_2 catalysts [36]. At the source-reported S/C ratio of 4.84 and 700 °C, ethanol conversion reached 100%, and both catalysts remained stable for almost 50 h on stream. However, temperature-programmed oxidation of the used samples showed greater carbon production on the Ni-based catalyst. The mechanistic analysis associated this

difference with a stronger contribution of ethanol dehydration and ethylene formation on Ni under the studied conditions [36]. Thus, comparable conversion and apparent stability did not correspond to identical carbon behavior.

6.2. Promoter and Support Chemistry: Suppressing Dehydration and Carbon Accumulation

The acid–base and redox properties of the support can alter the balance between reforming and coke-precursor formation. Osorio-Vargas et al. modified Ni/γ-Al_2O_3 with 15 wt.% La_2O_3 and different amounts of CeO_2 and combined catalytic testing with TEM, NH_3-TPD, XRD, TPR, XPS, DRIFTS, TPO-TG, and Raman characterization [37]. For the formulation containing 15 wt.% La_2O_3 and 10 wt.% CeO_2, the carbon-deposition rate was reduced by 72% relative to Ni supported on bare alumina. The authors attributed the improvement to lower selectivity toward ethylene following reduction of strong Lewis acid sites, together with carbon-removal contributions associated with lanthanum oxycarbonate formation and mobile lattice oxygen from CeO_2. The catalyst showed source-described good H_2 selectivity, no C_2 intermediates above 723 K, and stability for up to 48 h at 773 K [37]. Because the primary abstract does not provide a numerical H_2-selectivity value, no percentage is assigned to that descriptor in Table 5.

Table 5. Representative ESR catalyst evidence verified against primary publications. Metrics are retained in the source-reported form; rows are not a performance ranking.

Catalyst/Formulation	Source-Reported Conditions	Ethanol Conversion	H_2 Descriptor as Reported	Stability/Carbon Evidence	Ref.
Ni/MgO; Co/MgO	Simulated MCFC conditions; endurance at GHSV = 10,000 h^{-1}	n.r. in verified abstract	Ni/MgO: higher H_2 selectivity than Co/MgO (source comparison; no % restated)	630 h endurance test; coke strongly depressed by basic MgO	[34]
~12% Co/Al_2O_3, Co/SiO_2, Co/TiO_2; commercial Ni/Al_2O_3 benchmark	Atmospheric pressure; high-T comparison > 550 °C	Complete above 550 °C	H_2 yield approached 5 mol H_2/mol ethanol converted	Alumina-supported Co and Ni: acceptable deactivation rates but high carbon formation	[35]
La-promoted Ni/ZrO_2 and Co/ZrO_2	700 °C; source-reported S/C = 4.84	100%	Selectivity evaluated; exact numerical H_2 value not used in this audit	Stable for almost 50 h; TPO showed more carbon on Ni-based catalyst	[36]
Ni/γ-Al_2O_3 + 15 wt.% La_2O_3 + 10 wt.% CeO_2	Stability at 773 K (500 °C); C_2 species assessed vs. T	n.r. in verified abstract	Good H_2 selectivity (source wording; no % given in verified abstract)	Stable up to 48 h; carbon-deposition rate 72% lower than bare-Al_2O_3 catalyst; no C_2 intermediates above 723 K	[37]
8 wt.% Ni–Co/$MgAl_2O_4$–CeO_2; Co = 1, 3, or 5 wt.%	650 °C; 7 h	n.r. in verified abstract	Activity and H_2 selectivity favored for bimetallic catalysts; no % restated	7 h test; XRD did not resolve Ni, Co, or alloy peaks in reduced samples	[38]
RhPt/La_2O_3	600 °C; 21 mol.% H_2O + 3 mol.% ethanol; H_2O/EtOH = 7; GHSV > 55,000 h^{-1}	>99% throughout 120 h stability test	H_2/CO optimized; air regeneration increased H_2 selectivity (no % restated)	120 h TOS; small carbonaceous residue; air regeneration improved stability, H_2 treatment accelerated deactivation	[39]

Notes: GHSV, gas hourly space velocity; TOS, time-on-stream; n.r., not reported in the verified primary abstract/text used for this audit. The source-reported S/C value in Ref. [36] is retained without reinterpretation. Expressions such as "good H_2 selectivity" or "higher H_2 selectivity" are preserved as qualitative source statements when a numerical metric and its calculation basis were not directly verified.

This evidence is more defensible than a general statement that basic or oxygen-storage promoters always suppress coking. In the present review, promoter effects are therefore

reported only for the specific formulation and conditions demonstrated experimentally. Where a source provides carbon-deposition rates, post-reaction TPO/TGA, or time-on-stream behavior, those observations are retained separately from conversion or H_2 metrics.

6.3. Ni-Co Bimetallic and Perovskite-Derived Catalysts: Demonstrated Benefits and Evidence Boundaries

Bimetallic Ni-Co formulations are attractive because the second metal can modify reduction behavior, metal dispersion, surface ensembles, and product selectivity. However, the presence of both Ni and Co in a nominal composition does not by itself prove formation of a homogeneous alloy or a universal anti-coking mechanism. Romero C. et al. prepared 8 wt.% Ni catalysts containing 1, 3, or 5 wt.% Co on $MgAl_2O_4$-CeO_2 and evaluated them at 650 °C for 7 h [38]. The bimetallic catalysts showed favored catalytic activity and source-reported H_2 selectivity relative to the monometallic systems. At the same time, XRD did not resolve metallic Ni, Co, or an Ni-Co alloy in the reduced samples, which the authors interpreted as evidence that the metallic crystallites were below the approximately 5 nm XRD detection limit. Accordingly, this study supports a beneficial bimetallic effect for the tested materials, but it is not used here as stand-alone diffraction proof of alloy formation.

Perovskite-type oxides can also function as catalyst precursors rather than remaining as the catalytic phase throughout reduction and reforming. Zhao et al. prepared ZrO_2-supported $LaNi_{1-x}Co_xO_3$ precursors and reported that reduction produced highly dispersed Ni-Co alloy nanoparticles on ZrO_2 modified by La_2O_3 [40]. Within that specific catalyst series, the bimetallic materials showed high activity, high source-reported H_2 selectivity, very good stability, improved resistance to coking relative to the corresponding monometallic catalysts, and good resistance to sintering [40]. These relative conclusions are supported by the primary study. However, exact percentage values from the earlier version of this review are not restated here because the numerical metric basis was not verified from the primary abstract used in the present audit. Most importantly, the ESR result is not extrapolated to glycerol steam reforming.

6.4. Noble-Metal Benchmark: Long-Term Stability Under Defined Conditions

Noble-metal systems provide a useful benchmark for activity and durability, but they should be compared with non-noble catalysts only under explicitly stated conditions. Cobo et al. investigated $RhPt/La_2O_3$ at space velocities above 55,000 h^{-1} and identified 600 °C with 21 mol.% H_2O and 3 mol.% ethanol (H_2O/ethanol = 7) as conditions that maximized the H_2/CO ratio and reduced CH_4 while maintaining complete ethanol conversion [39]. A 120 h stability experiment under these conditions maintained ethanol conversion above 99% throughout the test. Regeneration experiments were also informative: H_2 treatment accelerated deactivation, whereas air regeneration increased catalyst stability and H_2 selectivity and decreased CH_4 generation. Post-reaction characterization showed partial oxidation of Rh and small amounts of carbonaceous residue [39]. This study demonstrates why long-term activity, regeneration response, and spent-catalyst characterization provide stronger evidence of durability than a short high-conversion test. The representative ESR catalyst performance and stability data discussed above are summarized in Table 5.

6.5. Evidence-Based Implications for ESR Catalyst Design

The verified primary evidence supports several feedstock-specific conclusions. First, support is an active determinant of ESR selectivity and deactivation: basic MgO can strongly suppress coke under the conditions studied by Freni et al. [34], whereas alumina-supported Co and Ni showed substantial carbon formation in the study of Bichon et al. [35]. Second, promoter combinations can simultaneously modify acid–base chemistry and carbon re-

moval; the La_2O_3/CeO_2-promoted Ni/Al_2O_3 system provides direct evidence through both catalytic and post-reaction characterization [37]. Third, Ni and Co can give similar conversion and time-on-stream behavior while producing different amounts of carbon, as shown on lanthanum-promoted zirconia [36]. Therefore, conversion alone is not a sufficient descriptor of catalyst durability.

Fourth, bimetallic Ni-Co systems show genuine promise for ESR, but the evidence must be stated at the level demonstrated. The $MgAl_2O_4$-CeO_2-supported series of Romero C. et al. supports improved activity and H_2 selectivity for bimetallic formulations [38], whereas the perovskite-derived system of Zhao et al. supports formation of a highly dispersed Ni–Co alloy after reduction together with improved coking and sintering resistance relative to the corresponding monometallic catalysts [40]. These findings justify discussion of Ni-Co/perovskite-derived materials as a promising ESR design strategy, but not as a universal catalyst platform for other feedstocks.

Finally, long-duration data remain essential for meaningful comparison. A 7 h screening test [38], an almost 50 h stability experiment [36], a 120 h test with regeneration interventions [39], and a 630 h endurance experiment [34] are different forms of evidence and are not treated as equivalent. Subsequent cross-feedstock discussion should therefore compare not only conversion and source-defined H_2 metrics but also duration, regeneration history, and direct evidence of carbon accumulation or structural change.

Recent ESR studies provide additional direct evidence that support-induced electronic structure and morphology control Co-based performance. Li et al. [41] reported 97% ethanol conversion and a source-defined H_2 yield of 73% for $Co/Si_4Al_2O_2N_6$, while XPS and in situ DRIFTS linked the improved behavior to stronger metal-support interaction, a lower Co valence state, and enhanced C-C bond cleavage. Lupa et al. [42] used a one-step hard-template method to prepare highly porous CeO_2 that generated smaller, more uniformly dispersed Co particles and reduced the severity of carbon-driven deactivation relative to a conventional CeO_2-supported comparison catalyst. These studies strengthen the argument that support morphology and electronic interaction should be evaluated together.

Promoter effects remain formulation-specific. Amini et al. [43] showed that 2 wt.% Y promotion of a Co-Ni catalyst on ordered mesoporous carbon increased particle dispersion and reduced carbon deposition; the authors reported excellent stability for the promoted formulation at 375 °C. The source also reports its own H_2-yield metric, but that percentage is not used here for cross-study ranking because its calculation basis differs from production-rate and selectivity descriptors used elsewhere.

Recent noble- and base-metal studies also extend the stability evidence. Zhao et al. [44] prepared $Rh\text{-}Ce/Al_2O_3$ catalysts in which CeO_2 trapped single-atom Rh species to form Rh-O-Ce sites; in situ DRIFTS-MS and isotopic kinetic analysis linked these sites to enhanced water activation, and the optimized catalyst reached a source-reported H_2 production rate of 22.4 mmol g^{-1} min^{-1} at 450 °C with remarkable stability. Grzybek et al. [45] reported two Co/Al_2O_3 design strategies that strengthened Co-Al interaction; the catalysts maintained 100% ethanol conversion for 21 h at 500 °C while the dehydration pathway was suppressed. These results are retained as source-specific evidence and are not converted to a common ranking metric.

7. Glycerol Steam Reforming: Catalyst Systems and Source-Verified Performance

Glycerol steam reforming (GSR) is the most demanding of the three feedstocks considered in this review because glycerol contains two C-C bonds and three hydroxyl groups and can generate a broad spectrum of oxygenated intermediates, methane, carbon oxides, and carbonaceous deposits. The reaction network and the thermodynamic limits were

discussed in Sections 3 and 4. The present section is therefore restricted to catalyst evidence that can be traced to primary experimental studies. As in the preceding sections, glycerol conversion, H_2 yield, H_2 selectivity, and gas-phase H_2 concentration are retained as distinct source-defined quantities and are not interconverted without a complete calculation basis [46–52].

A further complication specific to GSR is that catalyst stability can depend strongly on whether purified glycerol or crude biodiesel-derived glycerol is used. Consequently, high conversion obtained with an aqueous model feed does not establish tolerance toward methanol, salts, soaps, residual esters, or other components of crude glycerol. For this reason, evidence from purified and crude feeds is identified separately below, and catalyst claims are not transferred between the two feed types without direct testing.

The state of GSR catalysts before and after reaction is especially important because Ni and Co particles may sinter, oxidize/reduce, become partially covered by carbon, or emerge from oxide/perovskite precursors as phases that differ from the as-synthesized structure. The studies considered here therefore use spent-catalyst microscopy, diffraction, temperature-programmed oxidation, surface spectroscopy, and carbon characterization to distinguish precursor identity from the active or deactivated state [47–57]. This distinction is essential for perovskite-derived materials, for which reduction can collapse the parent lattice and generate supported metallic nanoparticles.

7.1. Ni-Based Catalysts: Support and Promoter Effects

Nichele et al. compared Ni supported on several oxides and found that the nature of the support strongly affected stability [47]. For Ni/ZrO_2, approximately 72% glycerol conversion and approximately 65% source-reported H_2 yield were retained after 20 h at 650 °C. The verified source excerpt does not provide a sufficiently explicit denominator to renormalize that percentage to mol H_2 per mol glycerol or to a theoretical-yield basis. The value is therefore preserved without conversion and is not directly compared with differently normalized H_2 metrics. The study nevertheless provides direct evidence that support–metal interaction influences time-on-stream behavior.

Nichele et al. compared Ni supported on several oxides and found that the nature of the support strongly affected stability [47]. For Ni/ZrO_2, approximately 72% glycerol conversion and approximately 65% source-reported H_2 yield were retained after 20 h at 650 °C. In contrast, other supports showed stronger deactivation under comparable tests. The study therefore provides direct evidence that support-metal interaction can influence not only initial activity but also time-on-stream behavior. The reported H_2 yield is retained on the basis used by the authors and is not converted into H_2 selectivity.

A more explicit demonstration of the effect of support basicity was reported by Charisiou et al. for 8 wt.% Ni on CaO-MgO-modified Al_2O_3 compared with Ni/Al_2O_3 [48]. Activity tests were carried out between 400 and 750 °C, and 20 h stability tests were performed at 600 °C with a water-to-glycerol molar feed ratio (WGFR) of 9:1. The modified support increased catalyst basicity and the surface fraction of Ni^0, favored conversion to gaseous products and H_2/CO_2 formation, and substantially improved time-on-stream stability relative to unmodified alumina. Post-reaction characterization further showed that the modifier decreased the amount of deposited carbon and shifted it toward less graphitic and more defective structures [48]. No single maximum H_2-yield value from this study is used here because the verified source summary does not provide a directly auditable value on the same basis as the stability test.

Yttria-stabilized zirconia provides a second example in which a promoter changes both metal stability and coke character. Charisiou et al. compared Ni/Y_2O_3-ZrO_2 with Ni/ZrO_2 and found that the Y_2O_3-containing catalyst retained a higher H_2 yield after 20 h

(2.17 versus 1.50 mol H_2 per mol glycerol) [49]. The same work showed substantially less Ni-particle sintering on the yttria-containing catalyst, while carbon on Ni/ZrO_2 was more graphitic and less readily oxidized. Thus, the total amount of carbon alone did not fully describe deactivation severity; carbon structure and metal sintering also mattered [49].

7.2. Crude Glycerol: Catalyst Performance Under a More Realistic Feed

Evidence obtained with crude glycerol is especially important for claims of practical robustness. Veiga and Bussi tested Ni supported on activated carbon at 650 °C using crude glycerol and examined promotion with MgO, La_2O_3, Y_2O_3, and Rh [50]. MgO promotion increased the H_2 yield to more than 80% of the theoretical maximum stated by the authors. However, carbon deposition and active-metal sintering remained the principal causes of deactivation. This study is used here as evidence that promoter benefits demonstrated with crude glycerol can coexist with significant deactivation mechanisms; it is not used to claim impurity tolerance for all Ni/MgO-containing catalysts.

7.3. Co-Based and Perovskite-Derived Catalysts: What Is Directly Demonstrated

Perovskite-derived catalysts require particularly careful terminology because the oxide precursor may not remain structurally intact during reduction. Surendar et al. prepared La-Ce-Co mixed oxides and evaluated the reduced materials in GSR between 500 and 700 °C at atmospheric pressure [51]. For the $La_{0.7}Ce_{0.3}CoO_3$ precursor, the perovskite structure collapsed during reduction, and Co metal became dispersed on a La_2O_3-CeO_2 mixed-oxide matrix. At 700 °C, the catalyst gave complete glycerol conversion and a source-reported H_2 yield of 68%; Co particles of approximately 4–5 nm were associated with low coke formation [51]. Accordingly, this material is described here as a perovskite-derived cobalt catalyst, not as an intact perovskite catalyst operating through a proven exsolution mechanism.

This distinction directly addresses an evidence gap identified during revision. The present source audit did not identify a GSR-specific primary publication that verifies the previously claimed quantitative performance of LaNi1-xCoxO3-derived Ni-Co, $La_{0.8}Sr_{0.2}Ni_{0.8}Co_{0.2}O_3$, or $BaNi_{0.75}Co_{0.25}O_3$ under glycerol steam-reforming conditions. Those compositions are therefore not included in the quantitative GSR table, and ESR evidence for Ni-Co/perovskite systems is not transferred to GSR. Any future inclusion of such compositions should require a glycerol-specific primary study with clearly defined performance metrics and reaction conditions.

7.4. Noble-Metal Benchmark and Stability Evidence

Rh-based catalysts provide a useful benchmark because they often suppress some of the kinetic limitations observed with base metals, although their cost and availability constrain large-scale use. Charisiou et al. compared Rh/gamma-Al_2O_3 catalysts modified with CeO_2, MgO, or La_2O_3 and conducted 12 h stability experiments at 600 °C with WGFR = 9:1 [52]. Across the tested formulations, total glycerol conversion remained approximately 90%, conversion to gaseous products was approximately 45%, and H_2 selectivity was approximately 78%; the final source-reported H_2 yield was 2.4–2.9 mol H_2 per mol glycerol. TEM analysis indicated largely amorphous carbon and limited sintering, which helped explain the observed stability [52]. These values are retained as a source-specific benchmark rather than used to rank Rh directly against Ni systems tested under different conditions. The representative GSR catalyst performance and stability data discussed above are summarized in Table 6.

Table 6. Representative GSR catalyst evidence verified against primary publications. Source-defined metrics are retained without conversion between H_2 yield, H_2 selectivity, and gas composition.

Catalyst/Formulation	Feed and Key Conditions	Glycerol Conversion	H_2 Metric as Reported	Stability/Deactivation Evidence	Ref.
Ni-ZrO_2/CeO_2	Purified glycerol; 700 °C; tubular fixed-bed reactor	Complete conversion	3.95 mol H_2/mol glycerol fed	Feed concentration, space time, temperature, and TOS evaluated	[46]
Ni/ZrO_2	Purified glycerol; 650 °C; 20 h test	~72% after 20 h	~65% H_2 yield (source-reported percentage; denominator not recoverable from verified source excerpt; retained without renormalization and not directly compared)	Support-dependent stability; Ni/ZrO_2 retained activity better than several comparisons supports	[47]
8 wt.% Ni/CaO-MgO-Al_2O_3	Parametric tests 400–750 °C; stability: 600 °C, WGFR 9:1, 20 h	Performance reported separately from the 20 h stability test	Improved H_2 production/selectivity relative to Ni/Al_2O_3; no single maximum value used here	20 h TOS showed markedly improved stability vs. Ni/Al_2O_3; lower carbon deposition with less graphitic/more defective carbon	[48]
Ni/Y_2O_3-ZrO_2	Purified glycerol; 20 h TOS comparison with Ni/ZrO_2	Source reports lower activity loss than Ni/ZrO_2	2.17 mol H_2/mol glycerol after 20 h vs. 1.50 for Ni/ZrO_2	Much less Ni sintering: carbon on Ni/ZrO_2 was more graphitic and harder to oxidize	[49]
Ni/activated carbon + MgO promoter	Crude glycerol; 650 °C	n.r. in verified abstract	>80% of theoretical H_2 amount (source wording)	Carbon deposition and metal sintering remained the main deactivation sources	[50]
La0.7Ce0.3CoO3-derived Co	Purified glycerol; 700 °C; atmospheric pressure	100%	68% H_2 yield	Perovskite collapsed on reduction; Co ~4–5 nm on La_2O_3-CeO_2; low coke formation	[51]
Rh/gamma-Al_2O_3 modified with CeO_2, MgO or La_2O_3	Purified glycerol; 600 °C; WGFR 9:1; 12 h	~90% total; ~45% to gaseous products	~78% H_2 selectivity; final H_2 yield 2.4–2.9 mol/mol	Stable over 12 h; largely amorphous carbon; sintering mostly avoided	[52]

Notes: WGFR, water-to-glycerol feed molar ratio; TOS, time-on-stream; n.r., not reported in the verified primary abstract/text used for this audit. Conditions from different experiments in the same paper are not merged into one operating point. Values reported as percentages and values reported as mol H_2/mol glycerol are intentionally kept in their original forms.

7.5. Evidence-Based Implications for GSR Catalyst Design

The verified GSR literature supports five conclusions. First, support chemistry strongly affects both activity and deactivation. ZrO_2-, CeO_2-containing, and basic mixed-oxide environments can improve the stability or product distribution of Ni catalysts, but the magnitude of the benefit is formulation-specific [46–49]. Second, promoter effects must be evaluated using direct time-on-stream and spent-catalyst evidence; reduced carbon quantity does not necessarily imply easier regeneration if the remaining carbon is more graphitic [49]. Third, crude-glycerol testing can reveal deactivation behavior that is not captured by purified model feeds [50].

Fourth, perovskite-derived systems should be described according to the structure actually present after reduction. For $La_{0.7}Ce_{0.3}CoO_3$, the primary study demonstrates collapse of the perovskite precursor and formation of dispersed Co on a La_2O_3-CeO_2 matrix [51]. It therefore does not justify a generic statement that intact perovskite lattices or controlled exsolution govern all GSR catalysts. Fifth, the present evidence base does not support extending the Ni–Co/perovskite strategy demonstrated in ESR to GSR as an established result. This limitation should remain explicit in the final comparative discussion and conclusion.

Recent GSR studies reinforce the importance of support chemistry while adding longer source-verified stability tests. Macedo et al. [53] reported that $NiAlLaO_x$ gave 91% glycerol conversion to gaseous products and an H_2 yield of 5.40 mol H_2 per mol glycerol at 700 °C; a separate 24 h stability test at 625 °C showed stable behavior with low coke formation, which the authors related in part to $LaAlO_3$-containing support chemistry and strong Ni-support interaction. Wang et al. [54] compared rapid and conventional calcination of Ni/CeO_2 and showed that rapid calcination strengthened $Ni\text{-}CeO_2$ interaction and increased oxygen-vacancy formation, improving stability and suppressing carbon deposition. These results provide current primary evidence that preparation history can alter oxygen-storage behavior and sintering/coking resistance in GSR.

The current literature also expands the range of directly demonstrated GSR precursor/support structures. Reynoso et al. [55] evaluated cobalt-aluminate-spinel-derived catalysts at 550 °C and showed that Co/Al ratio and space-time strongly affected carbon-to-gas conversion and H_2 selectivity; deactivation/regeneration analysis identified cobalt leaching and predominantly amorphous carbon under severe conditions. More importantly for the perovskite discussion, Luisetto et al. [56] directly tested Ni supported on $CaZrO_3$, $SrZrO_3$, and $BaZrO_3$ in GSR. $Ni/SrZrO_3$ produced >6 mol H_2 per mol glycerol above 500 °C and showed strong time-on-stream stability; structural evidence supported reduction-driven exsolution of Ni species incorporated into the perovskite lattice. This is direct GSR evidence for a Ni/perovskite-support strategy, but it does not establish the previously claimed Ni-Co dual-metal perovskite platform.

A 2026 study by Wang et al. [57] demonstrated a distinct alloy/promoter route: Ni_3Mo supported on a Mo-modified attapulgite-based zeolite reached 95.3% glycerol conversion and a source-defined H_2 yield of 77.3% and maintained superior stability for 50 h at 600 °C. The authors associated the performance with Ni-Mo alloy formation, abundant oxygen vacancies, reduced strong acidity, and suppression of Ni sintering and carbon deposition. The percentage H_2 yield is retained on the source basis and is not converted into mol H_2 per mol glycerol.

8. Comparative Synthesis, Evidence Gaps, and Research Priorities

The preceding sections show that methanol, ethanol, and glycerol should be compared as related but chemically distinct steam-reforming systems rather than as interchangeable members of one catalyst platform. Their balanced overall reactions provide stoichiometric H_2 maxima of 3, 6, and 7 mol H_2 per mol feed, respectively, but the increasing number of C–C bonds and oxygen-containing functional groups from methanol to glycerol also increases the number of possible intermediates, competing pathways, and deactivation routes. Consequently, catalyst design must be matched to the feedstock-specific reaction network and to the operating conditions under which the catalyst is evaluated [1–3].

8.1. Expanded Evidence Base: Complementary Studies Beyond the Quantitative Tables

The expanded literature set was used to deepen mechanistic and catalyst-design coverage without enlarging the quantitative tables with non-comparable performance maxima. Established deactivation frameworks distinguish poisoning, fouling, or carbon deposition; thermal degradation and sintering; and structural or chemical transformations as mechanistically different causes of activity loss [58,59]. For nickel steam-reforming catalysts specifically, activity, sulfur poisoning, carbon formation, and sintering have long been recognized as separate design challenges [60]. Mechanistic interpretation is strongest when catalyst structure and activity are observed under the same reactive state; this principle underlies the operando methodology that combines in situ spectroscopy with simultane-

ous performance measurements [61]. These concepts provide a common framework for interpreting the feedstock-specific stability evidence summarized in Sections 5–7.

Additional MSR studies reinforce the conclusion that selectivity and stability are controlled by formulation and interfacial chemistry rather than by nominal Cu loading alone. $CuPd/ZrO_2$ has been used to isolate the influence of surface composition on methanol conversion and CO selectivity [62], while CeO_2- and ZrO_2-promoted $Cu–ZnO/Al_2O_3$ systems further demonstrate strong support and promoter effects [63]. Kinetic and catalyst-composition studies on $Cu/ZnO/Al_2O_3$ and ZrO_2/Al_2O_3-promoted formulations specifically address CO formation and its suppression [64–66]. Non-Cu systems provide an important mechanistic contrast: ZnO-supported Ni, Co, Pd, and Pt catalysts [67] and Pd/ZnO [68] established the relevance of metal–Zn interactions, whereas reactive transformation of intermetallic In–Pt compounds represents a distinct high-selectivity MSR strategy [69]. Statistical optimization of $CuO–ZnO/Al_2O_3$ composition also links Cu/Zn content, Cu dispersion, and deactivation by sintering [70]. Together, these studies broaden the MSR evidence base while supporting the decision not to rank catalysts across dissimilar metric definitions and reactor conditions.

For ESR, a substantial body of foundational primary work complements the smaller set retained in Table 5. Supported Co catalysts show pronounced support dependence [71], and in situ DRIFT–mass spectrometry has directly followed surface intermediates over Co/ZnO under reforming conditions [72]. Co crystallite size [73] and synthesis/support history [74] also alter activity and selectivity. Ni-based reaction-network analysis provides a mechanistic basis for the competing acetaldehyde-, ethylene-, methane-, and carbon-forming branches discussed in Section 3 [75]. Additional cobalt studies address catalyst formulation, activity, and stability [76,77], while cross-metal comparisons demonstrate the strong dependence of ESR on both active metal and support [78]. The broader ESR literature also includes a critical process/catalyst synthesis [79], low- and intermediate-temperature experiments [80], structural studies of $NiO–CeO_2–ZrO_2$ [81], and direct mechanistic evidence for complementary roles of Ni and CeO_2 in Ni/CeO_2 [82]. These studies support a feedstock-specific ESR design framework rather than a single universal reaction sequence.

The GSR evidence base is similarly strengthened by earlier and complementary studies that span realistic feed valorization, active-metal selection, support chemistry, and reactor intensification. Steam reforming of biodiesel by-product glycerol was demonstrated directly in early process-oriented work [83], while Ru [84], Ni catalysts [85,86], Pt catalysts [87], and an additional Ni study [88] established multiple viable catalytic routes. Support and precursor effects have been examined through La_2O_3 modification [89], $La_{1-x}Ce_xNiO_3$-derived materials [90], and ceria-supported metal catalysts [91]. Sorption-enhanced GSR illustrates how in situ CO_2 capture can be integrated with the reforming reaction [92]. Catalyst-preparation effects are further demonstrated by N_2O-mediated calcination of $Ni/\gamma\text{-}Al_2O_3$ [93], while Ni–Cu and Ni–Co catalysts on La–Mg mixed oxides extend the bimetallic GSR literature without justifying transfer of ESR perovskite claims to glycerol [94]. A Pt/SiO_2-C system additionally illustrates how support architecture can influence GSR behavior [95]. Because these publications employ heterogeneous definitions of H_2 performance and different operating conditions, they are integrated here as complementary evidence rather than merged into a single numerical ranking.

A targeted update of the 2024–2025 literature further strengthens the contemporary evidence base. For MSR, porous Cu/CeO_2 with abundant $Cu^+–O_v–Ce^{3+}$ interfacial sites links water activation and hydrogen production to a defined metal–support interface [96]. For ESR, recyclable $NiCaO_x$/NaCl catalysts [97], a Ni–Al spinel-derived catalyst examined across reaction and deactivation regimes [98], and a multifunctional $NiCoMnCeCaO_x$ nanorod [99] provide recent examples of how active-phase chemistry, regeneration, and

carbon tolerance are being addressed. For GSR, support-dependent Ni catalysts studied in 2025 directly connect hydrogen production, stability, and carbon deposition behavior [100]. These additions complement, rather than replace, the source-verified comparisons above and increase the representation of current primary research.

8.2. Feedstock-Specific Catalyst Functions

For MSR, the verified literature places particular emphasis on low-temperature methanol activation, Cu dispersion and reducibility, control of CO-forming pathways, and preservation of the Cu-support interface [20–28]. Cu/Zn/Al, Cu/CeO_2, Cu/ZrO_2, and related composite systems can all perform effectively, but the evidence reviewed in Section 5 does not support identification of one universal Cu oxidation state, support, or preparation method as optimal under all conditions. Support chemistry changes reduction behavior, interfacial structure, selectivity, and time-on-stream stability, and these effects must be evaluated within the specific catalyst architecture.

For ESR, the principal catalytic requirement shifts toward a balance between C–C bond transformation and suppression of dehydration, methane formation, and carbon accumulation. Ni and Co remain important non-noble active metals, while basic and redox-active supports can modify the probability of ethylene formation and the removal of surface carbon [34–37]. The source-verified Ni–Co literature supports a beneficial bimetallic effect in selected ESR systems, and the $LaNi_{1-x}Co_xO_3$-derived catalyst investigated by Zhao et al. provides direct evidence for a perovskite-derived Ni–Co alloy formulation with improved coking and sintering resistance relative to the corresponding monometallic materials [38,40]. This evidence is meaningful for ESR, but it is not a basis for assuming equivalent behavior in GSR.

For GSR, catalyst requirements are broader because C3 oxygenated intermediates, methane formation, and carbon deposition must be controlled simultaneously. The primary studies reviewed in Section 7 show that support basicity, redox properties, metal-support interaction, and resistance to Ni sintering can all influence stability [46–52]. Crude-glycerol experiments further demonstrate that feed impurities can expose deactivation behavior that is not necessarily captured using purified glycerol [50]. Perovskite-derived cobalt systems are promising, but the structure present after reduction must be described accurately. In the $La_{0.7}Ce_{0.3}CoO_3$ case, the primary study supports formation of dispersed Co on a La_2O_3-CeO_2 matrix after collapse of the precursor rather than operation of an intact perovskite lattice [51].

8.3. Stability and Deactivation as Primary Performance Criteria

A consistent finding across the three feedstocks is that initial conversion is not an adequate measure of catalyst quality. In MSR, deactivation may arise from changes in the Cu-containing phase, loss of interfacial structure, or support-dependent changes in the active surface [22–24]. In ESR and GSR, carbon deposition becomes increasingly important, but even here the amount of deposited carbon is not the only relevant variable. Carbon structure, oxidizability, metal sintering, support acidity, promoter mobility, and regeneration history can determine whether a catalyst retains useful activity [34–40,46–52].

The evidence also shows that stability claims are not directly comparable when they originate from experiments of different duration or design. A short screening test, a stable interval within a longer experiment, a regeneration cycle, and a post-reaction coke analysis answer different questions. For this reason, the present review treats time-on-stream, regeneration behavior, and spent-catalyst characterization as independent descriptors. Future comparative studies would be more informative if activity profiles, carbon measurements,

particle-size evolution, and changes in oxidation state were reported together rather than summarized by a single statement that a catalyst was 'stable'.

8.4. Performance Metrics and the Need for Source-Level Traceability

The most important methodological lesson from the source audit is that conversion, H_2 yield, H_2 selectivity, and dry-gas H_2 concentration cannot be combined into a common percentage without changing the meaning of the original data. Differences in normalization basis are especially consequential when feed conversion is incomplete. Furthermore, water-to-feed ratio and carbon-normalized S/C are numerically different for ethanol and glycerol, as defined in Section 4. Direct rankings based on the largest percentage in a table are therefore not scientifically defensible unless the metric definition and operating basis are equivalent.

For future reviews and experimental studies, source traceability should be treated as part of the scientific result. A catalyst-performance table is most useful when each numerical entry can be traced to the primary paper, the original metric definition, and the corresponding temperature, pressure, feed composition, steam ratio, space velocity, catalyst mass, reactor configuration, and time-on-stream. In the present revision, Supplementary Table S1 provides this link for the retained quantitative entries. Verification status is identified explicitly: full-text checks are distinguished from abstract-only or limited-source verification, and values lacking a recoverable normalization basis are retained only with that limitation and are excluded from direct numerical ranking.

8.5. Research Priorities

Several priorities emerge from the verified evidence. First, catalyst studies should move beyond isolated maximum conversion values toward long-duration experiments with simultaneous reporting of H_2 production, carbon balance, coke quantity and character, metal-particle evolution, and regeneration response. This is particularly important for ESR and GSR, where high conversion can coexist with substantial carbon formation [35,36,48,49].

Second, mechanistic claims should increasingly be supported by in situ or operando characterization under actual steam-reforming conditions. Terms such as alloy formation, exsolution, oxygen-vacancy-mediated carbon removal, strong metal-support interaction, and Mars-van Krevelen behavior describe distinct physical processes and should not be used interchangeably. The revised evidence base supports some of these assignments for specific catalysts, but not as universal mechanisms across MSR, ESR, and GSR.

Third, more ESR and especially GSR studies should use realistic feed compositions. For glycerol, direct comparison of purified and crude feeds is needed to separate intrinsic catalyst activity from tolerance toward salts, residual methanol, soaps, esters, and other biodiesel-derived impurities. For ethanol and methanol, similarly rigorous evaluation of water content and relevant trace contaminants would improve the connection between laboratory performance and process operation.

Fourth, catalyst comparison should be integrated more closely with reactor and process constraints. A catalyst that requires very high steam dilution may suppress coke but impose a large vaporization and heating duty; conversely, a catalyst that performs at a lower steam ratio may be attractive only if stability is maintained. Future work should therefore report catalytic performance together with steam demand, pressure, space velocity, heat-management requirements, and product-gas quality. Such integration is necessary before catalyst-level advantages can be translated into process-level conclusions.

Finally, the evidence gap surrounding Ni–Co/perovskite strategies in GSR should be treated as a research opportunity rather than filled by analogy. The ESR literature demonstrates that carefully designed Ni–Co and perovskite-derived systems can be ef-

fective [38,40], whereas the GSR literature verified here does not yet provide equivalent primary evidence for the same dual-metal perovskite compositions. Glycerol-specific synthesis, reduction, operando characterization, long-term testing, and carbon analysis are therefore needed before a cross-feedstock catalyst platform can be claimed.

9. Conclusions

This review provides a source-verified comparison of catalytic steam reforming of methanol, ethanol, and glycerol with emphasis on reaction chemistry, catalyst design, performance metrics, and deactivation. The central conclusion is that the three feedstocks should not be described by a single generalized reaction mechanism or evaluated through a single catalyst-performance metric. Methanol, ethanol, and glycerol differ systematically in carbon number, C-C bond content, functional-group density, reaction-network complexity, and susceptibility to carbon-forming pathways. Their stoichiometric maxima of 3, 6, and 7 mol H_2 per mol feed are therefore useful reference limits, but they are not experimental catalyst yields and do not identify the best practical feedstock or catalyst.

For methanol steam reforming, the strongest verified evidence supports Cu-containing catalysts whose performance is controlled by preparation method, Cu dispersion and reducibility, oxide-support chemistry, and the stability of the Cu-support interface. The principal catalytic challenge is the simultaneous achievement of high methanol conversion and favorable product distribution while limiting CO formation and preserving the active Cu-containing surface. The reviewed data show that CeO_2, ZrO_2, mesoporous supports, microstructured reactors, and selected promoters can improve specific aspects of performance, but their effects remain formulation- and condition-dependent. Recent 2024–2026 primary studies further support a dynamic interfacial picture in which Cu^+/Cu^0 functions and ZnO_x/Cu electronic interactions change under reaction conditions.

For ethanol steam reforming, C-C bond transformation introduces a substantially broader network involving acetaldehyde, ethylene, methane, carbon oxides, and carbonaceous deposits. Ni- and Co-based systems can provide high activity, while support basicity and redox functionality can suppress dehydration-derived coke precursors or assist carbon removal. The verified evidence also supports Ni-Co bimetallic and perovskite-derived strategies as promising for ESR. However, these conclusions apply to the specific ethanol systems in which they were demonstrated and should not be transferred automatically to glycerol reforming. Recent Co-, Co-Ni-, and Rh-based studies likewise reinforce the importance of support morphology, metal-support interaction, promoter effects, and explicitly reported time-on-stream stability.

For glycerol steam reforming, the dominant challenge is the simultaneous control of a complex C3 oxygenate network, methane formation, carbon deposition, and metal sintering. Ni-based catalysts remain attractive because of their activity for C–C bond transformation, but their stability depends strongly on the support and promoter environment. Primary studies support beneficial effects of ZrO_2-, CeO_2-containing, basic mixed-oxide, and yttria-stabilized supports in specific formulations. Crude-glycerol testing further shows that practical catalyst robustness must be evaluated in the presence of realistic impurities. Perovskite-derived cobalt catalysts can also be effective, but the reduced catalyst structure must be identified experimentally rather than inferred from the precursor formula. Recent 2024–2026 GSR studies provide direct evidence for $NiAlLaO_x$, Ni/CeO_2, cobalt-spinel-derived, Ni/perovskite-support, and Ni-Mo formulations; importantly, the Ni/perovskite evidence does not by itself establish a universal Ni-Co dual-metal perovskite platform.

A second major conclusion concerns data comparability. Feedstock conversion, H_2 yield, H_2 selectivity, and dry-gas H_2 concentration describe different quantities. Reclassifying one as another can create artificial performance rankings and was therefore avoided in

this review. The same caution applies to steam ratios: water-to-feed and carbon-normalized S/C must be distinguished for C2 and C3 oxygenates. Consequently, no catalyst is identified here as universally superior on the basis of a single maximum percentage. Performance should instead be interpreted within the original metric definition, reactor conditions, feed composition, and duration of the experiment.

The evidence reviewed also demonstrates that catalyst stability must be treated as a primary performance dimension. Time-on-stream behavior, carbon quantity and structure, metal sintering, oxidation-state changes, and regeneration response provide complementary information and should be reported together whenever possible. Thermodynamic equilibrium calculations remain valuable for identifying accessible product regions and carbon-forming tendencies, but they cannot substitute for experimental deactivation measurements.

Overall, the most defensible pathway for future progress is not a universal catalyst formulation for all three feedstocks, but a feedstock-specific design strategy supported by directly comparable and traceable primary data. For MSR, this means controlling Cu-based interfacial chemistry and CO formation; for ESR, balancing C–C activation with suppression of dehydration and carbon accumulation; and for GSR, combining C–C cleavage activity with robust control of oxygenated intermediates, methane, sintering, carbon formation, and realistic-feed impurities. Cross-feedstock catalyst concepts, including Ni–Co/perovskite-derived materials, should be presented as hypotheses for targeted validation where direct primary evidence is still absent. Applying these evidence and reporting standards should make future catalyst comparisons more reproducible and better aligned with eventual process-scale hydrogen production.

Supplementary Materials: The following supporting information can be downloaded at: https://www.mdpi.com/article/10.3390/catal16100920/s1. Supplementary Table S1: Source-verification and traceability matrix for the cited publications, including the quantitative entries retained in Tables 3–6 and their verification status; Supplementary Note S1: Detailed literature-search and source-verification procedure; Supplementary List S1: Abbreviations used in the Supplementary Information.

Author Contributions: Conceptualization, S.N. and B.M.; methodology, S.N.; investigation, S.N., T.B., B.M., R.O. and M.Y.; literature review and source verification, S.N., T.B., B.M., R.O. and M.Y.; writing—original draft preparation, S.N.; writing—review and editing, S.N., T.B., B.M., R.O. and M.Y.; visualization, S.N.; supervision, B.M.; project administration, S.N. and B.M. All authors have read and agreed to the published version of the manuscript.

Funding: This research was funded by the Science Committee of the Ministry of Science and Higher Education of the Republic of Kazakhstan, grant number AP25794455.

Data Availability Statement: No new experimental datasets were generated in this review. The source-verification and traceability information supporting the comparative tables is provided in Supplementary Table S1.

Acknowledgments: During manuscript preparation, the authors used generative-AI tools (Claude, (version claude-sonnet-4-6), Anthropic, and ChatGPT, OpenAI) for English-language editing, phrasing, structural organization, and consistency checking. These tools were not used to generate experimental data or to make autonomous study-inclusion decisions. All chemical equations, numerical values, catalyst-performance data, interpretations, and bibliographic entries were checked by the authors against the cited literature. The authors reviewed and edited all AI-assisted output and take full responsibility for the content of this publication.

Conflicts of Interest: The authors declare no conflicts of interest.

Abbreviations

The following abbreviations are used in this manuscript:

Abbreviation	Definition
ESR	ethanol steam reforming
GSR	glycerol steam reforming
MSR	methanol steam reforming
GHSV	gas hourly space velocity
WHSV	weight hourly space velocity
OSC	oxygen storage capacity
S/C	steam-to-carbon molar ratio
TOS	time-on-stream
TGA	thermogravimetric analysis
TPO	temperature-programmed oxidation
TPR	temperature-programmed reduction
WGFR	water-to-glycerol feed molar ratio
WGS	water–gas shift
XRD	X-ray diffraction
XPS	X-ray photoelectron spectroscopy

References

1. Bagnato, G.; Iulianelli, A.; Sanna, A.; Basile, A. Glycerol Production and Transformation: A Critical Review with Particular Emphasis on Glycerol Reforming Reaction for Producing Hydrogen in Conventional and Membrane Reactors. *Membranes* **2017**, *7*, 17. [CrossRef] [PubMed]
2. Ogo, S.; Sekine, Y. Recent Progress in Ethanol Steam Reforming Using Non-Noble Transition Metal Catalysts: A Review. *Fuel Process. Technol.* **2020**, *199*, 106238. [CrossRef]
3. Bepari, S.; Kuila, D. Steam Reforming of Methanol, Ethanol and Glycerol over Nickel-Based Catalysts-A Review. *Int. J. Hydrogen Energy* **2020**, *45*, 18090–18113. [CrossRef]
4. Peppley, B.A.; Amphlett, J.C.; Kearns, L.M.; Mann, R.F. Methanol–Steam Reforming on $Cu/ZnO/Al_2O_3$. Part 1: The Reaction Network. *Appl. Catal. A Gen.* **1999**, *179*, 21–29. [CrossRef]
5. Peppley, B.A.; Amphlett, J.C.; Kearns, L.M.; Mann, R.F. Methanol–Steam Reforming on $Cu/ZnO/Al_2O_3$ Catalysts. Part 2. A Comprehensive Kinetic Model. *Appl. Catal. A Gen.* **1999**, *179*, 31–49. [CrossRef]
6. Mathure, P.V.; Ganguly, S.; Patwardhan, A.V.; Saha, R.K. Steam Reforming of Ethanol Using a Commercial Nickel-Based Catalyst. *Ind. Eng. Chem. Res.* **2007**, *46*, 8471–8479. [CrossRef]
7. Gu, T.; Zhu, W.; Yang, B. Ethanol Steam Reforming on Rh: Microkinetic Analyses on the Complex Reaction Network. *Catal. Sci. Technol.* **2021**, *11*, 7009–7017. [CrossRef]
8. Cheng, C.K.; Foo, S.Y.; Adesina, A.A. Glycerol Steam Reforming over Bimetallic $Co-Ni/Al_2O_3$. *Ind. Eng. Chem. Res.* **2010**, *49*, 10804–10817. [CrossRef]
9. Sanchez, E.A.; Comelli, R.A. Hydrogen by Glycerol Steam Reforming on a Nickel–Alumina Catalyst: Deactivation Processes and Regeneration. *Int. J. Hydrogen Energy* **2012**, *37*, 14740–14746. [CrossRef]
10. Chiodo, V.; Freni, S.; Galvagno, A.; Mondello, N.; Frusteri, F. Catalytic Features of Rh and Ni Supported Catalysts in the Steam Reforming of Glycerol to Produce Hydrogen. *Appl. Catal. A Gen.* **2010**, *381*, 1–7. [CrossRef]
11. Adhikari, S.; Fernando, S.; Haryanto, A. A Comparative Thermodynamic and Experimental Analysis on Hydrogen Production by Steam Reforming of Glycerin. *Energy Fuels* **2007**, *21*, 2306–2310. [CrossRef]
12. Adhikari, S.; Fernando, S.; Haryanto, A. Production of Hydrogen by Steam Reforming of Glycerin over Alumina-Supported Metal Catalysts. *Catal. Today* **2007**, *129*, 355–364. [CrossRef]
13. Faungnawakij, K.; Kikuchi, R.; Eguchi, K. Thermodynamic Evaluation of Methanol Steam Reforming for Hydrogen Production. *J. Power Sources* **2006**, *161*, 87–94. [CrossRef]
14. Garcia, E.; Laborde, M. Hydrogen Production by the Steam Reforming of Ethanol: Thermodynamic Analysis. *Int. J. Hydrogen Energy* **1991**, *16*, 307–312. [CrossRef]
15. Vasudeva, K.; Mitra, N.; Umasankar, P.; Dhingra, S.C. Steam Reforming of Ethanol for Hydrogen Production: Thermodynamic Analysis. *Int. J. Hydrogen Energy* **1996**, *21*, 13–18. [CrossRef]

16. Lima Da Silva, A.; Malfatti, C.D.F.; Müller, I.L. Thermodynamic Analysis of Ethanol Steam Reforming Using Gibbs Energy Minimization Method: A Detailed Study of the Conditions of Carbon Deposition. *Int. J. Hydrogen Energy* **2009**, *34*, 4321–4330. [CrossRef]
17. Adhikari, S.; Fernando, S.; Gwaltney, S.; Filipto, S.; Markbricka, R.; Steele, P.; Haryanto, A. A Thermodynamic Analysis of Hydrogen Production by Steam Reforming of Glycerol. *Int. J. Hydrogen Energy* **2007**, *32*, 2875–2880. [CrossRef]
18. Rossi, C.; Alonso, C.; Antunes, O.; Guirardello, R.; Cardozofilho, L. Thermodynamic Analysis of Steam Reforming of Ethanol and Glycerine for Hydrogen Production. *Int. J. Hydrogen Energy* **2009**, *34*, 323–332. [CrossRef]
19. Díaz Alvarado, F.; Gracia, F. Steam Reforming of Ethanol for Hydrogen Production: Thermodynamic Analysis Including Different Carbon Deposits Representation. *Chem. Eng. J.* **2010**, *165*, 649–657. [CrossRef]
20. Lindström, B.; Pettersson, L.J.; Govind Menon, P. Activity and Characterization of Cu/Zn, Cu/Cr and Cu/Zr on γ-Alumina for Methanol Reforming for Fuel Cell Vehicles. *Appl. Catal. A Gen.* **2002**, *234*, 111–125. [CrossRef]
21. Shen, J.-P.; Song, C. Influence of Preparation Method on Performance of Cu/Zn-Based Catalysts for Low-Temperature Steam Reforming and Oxidative Steam Reforming of Methanol for H_2 Production for Fuel Cells. *Catal. Today* **2002**, *77*, 89–98. [CrossRef]
22. Tonelli, F.; Gorriz, O.; Tarditi, A.; Cornaglia, L.; Arrúa, L.; Cristina Abello, M. Activity and Stability of a CuO/CeO_2 Catalyst for Methanol Steam Reforming. *Int. J. Hydrogen Energy* **2015**, *40*, 13379–13387. [CrossRef]
23. Oguchi, H.; Nishiguchi, T.; Matsumoto, T.; Kanai, H.; Utani, K.; Matsumura, Y.; Imamura, S. Steam Reforming of Methanol over $Cu/CeO_2/ZrO_2$ Catalysts. *Appl. Catal. A Gen.* **2005**, *281*, 69–73. [CrossRef]
24. Abrokwah, R.Y.; Deshmane, V.G.; Kuila, D. Comparative Performance of M-MCM-41 (M: Cu, Co, Ni, Pd, Zn and Sn) Catalysts for Steam Reforming of Methanol. *J. Mol. Catal. A Chem.* **2016**, *425*, 10–20. [CrossRef]
25. Taghizadeh, M.; Abbandanak, M.H. Production of Hydrogen via Methanol Steam Reforming over Mesoporous CeO_2–Cu/KIT-6 Nanocatalyst: Effects of Polar Aprotic Tetrahydrofuran Solvent and ZrO_2 Promoter on Catalytic Performance. *Int. J. Hydrogen Energy* **2022**, *47*, 16362–16374. [CrossRef]
26. Khani, Y.; Safari, N.; Kamyar, N.; Bahadoran, F.; Torabi, M. High H_2 Selectivity with Low Coke Formation for Methanol Steam Reforming over $Cu/Y_{1.5}Ce_{0.84}Ru_{0.04}O_4$ Catalyst in a Microchannel Plate Reactor. *Int. J. Hydrogen Energy* **2022**, *47*, 971–983. [CrossRef]
27. Zhou, F.; Zhang, R.; Li, H.; Liu, J.; Wu, Y.; Toan, S.; Sun, Z. The Critical Role of Ga Doped Cu/Al_2O_3 Aerogels in Carbon Monoxide Suppression during Steam Reforming of Methanol. *Fuel Process. Technol.* **2023**, *249*, 107792. [CrossRef]
28. Ploner, K.; Watschinger, M.; Kheyrollahi Nezhad, P.D.; Götsch, T.; Schlicker, L.; Köck, E.-M.; Gurlo, A.; Gili, A.; Doran, A.; Zhang, L.; et al. Mechanistic Insights into the Catalytic Methanol Steam Reforming Performance of Cu/ZrO_2 Catalysts by in Situ and Operando Studies. *J. Catal.* **2020**, *391*, 497–512. [CrossRef]
29. Zhang, Q.; Li, D.; Jiang, Z.; Gu, H.; Zhu, M.; Jin, S.; Zhu, M. Structure-Activity Relationships of Zirconium-Modified Copper-Based Catalysts during Methanol Steam Reforming. *J. Catal.* **2024**, *436*, 115584. [CrossRef]
30. Song, M.; Li, L.; Wu, X.; Cai, H.; Li, G.; Hu, C. The Influence of the ZrO_2 Crystal Phase on Cu/ZrO_2-Al_2O_3 Catalysts in Methanol Steam Reforming. *Catalysts* **2024**, *14*, 480. [CrossRef]
31. Ma, J.; Mao, L.; Du, H.; Zhong, J.; Jiang, L.; Liu, X.; Xu, J.; Xu, X.; Fang, X.; Wang, X. Tracking the Critical Roles of Cu^+ and Cu^0 Sites and the Optimal Cu^+/Cu^0 Ratio for CH_3OH Steam Reforming to Manufacture H_2. *Chem. Eng. J.* **2024**, *496*, 154195. [CrossRef]
32. Liu, D.; Zhang, M.; Zhao, L.; Guo, X.; Xu, G.; He, H. Mechanistic Insights into Methanol Steam Reforming on Copper Catalysts: Dynamics of Active Sites and Reaction Pathway. *J. Catal.* **2025**, *442*, 115922. [CrossRef]
33. Liu, D.; Zhang, M.; Zhao, L.; Xu, G.; He, H. Electronic Metal-Support Interaction at ZnO_x/Cu Interface Enhances H_2 Production in Methanol Steam Reforming. *J. Am. Chem. Soc.* **2026**, *148*, 10764–10775. [CrossRef] [PubMed]
34. Freni, S.; Cavallaro, S.; Mondello, N.; Spadaro, L.; Frusteri, F. Production of Hydrogen for MC Fuel Cell by Steam Reforming of Ethanol over MgO Supported Ni and Co Catalysts. *Catal. Commun.* **2003**, *4*, 259–268. [CrossRef]
35. Bichon, P.; Haugom, G.; Venvik, H.J.; Holmen, A.; Blekkan, E.A. Steam Reforming of Ethanol Over Supported Co and Ni Catalysts. *Top. Catal.* **2008**, *49*, 38–45. [CrossRef]
36. Padilla, R.; Benito, M.; Rodríguez, L.; Serrano, A.; Muñoz, G.; Daza, L. Nickel and Cobalt as Active Phase on Supported Zirconia Catalysts for Bio-Ethanol Reforming: Influence of the Reaction Mechanism on Catalysts Performance. *Int. J. Hydrogen Energy* **2010**, *35*, 8921–8928. [CrossRef]
37. Osorio-Vargas, P.; Flores-González, N.A.; Navarro, R.M.; Fierro, J.L.G.; Campos, C.H.; Reyes, P. Improved Stability of Ni/Al_2O_3 Catalysts by Effect of Promoters (La_2O_3, CeO_2) for Ethanol Steam-Reforming Reaction. *Catal. Today* **2016**, *259*, 27–38. [CrossRef]
38. Romero C., L.; Moreno, M.S.; Galetti, A.E.; Barroso, M.N. Ni–Co Bimetallic Catalysts for Hydrogen Production by Steam Reforming Ethanol. *Top. Catal.* **2022**, *65*, 1427–1439. [CrossRef]
39. Cobo, M.; Pieruccini, D.; Abello, R.; Ariza, L.; Córdoba, L.F.; Conesa, J.A. Steam Reforming of Ethanol over Bimetallic $RhPt/La_2O_3$: Long-Term Stability under Favorable Reaction Conditions. *Int. J. Hydrogen Energy* **2013**, *38*, 5580–5593. [CrossRef]

40. Zhao, L.; Han, T.; Wang, H.; Zhang, L.; Liu, Y. Ni-Co Alloy Catalyst from $LaNi_{1-x}Co_xO_3$ Perovskite Supported on Zirconia for Steam Reforming of Ethanol. *Appl. Catal. B Environ.* **2016**, *187*, 19–29. [CrossRef]
41. Li, L.; Li, R.; Xu, J.; Liu, Y.; Lu, L. $Si_4Al_2O_2N_6$ Regulating Chemical States of Co Catalyst for Improved Hydrogen Production from Ethanol Steam Reforming. *Int. J. Hydrogen Energy* **2024**, *57*, 738–745. [CrossRef]
42. Lupa, J.; Greluk, M.; Rotko, M.; Słowik, G.; Sienkiewicz, A.; Kierys, A. Ethanol Steam Reforming for Hydrogen Production over Cobalt Catalyst Supported on the Cerium Oxide Prepared via the One-Step Hard Template Method. *Chem. Eng. J.* **2024**, *499*, 156101. [CrossRef]
43. Amini, V.; Shahed Gharahshiran, V.; Yousefpour, M. Hydrogen Production via Ethanol Steam Reforming over Yttrium-Modified Co-Ni Catalysts: The Role of Promoter. *Heliyon* **2025**, *11*, e43032. [CrossRef]
44. Zhao, L.; Liu, D.; Wang, Y.; Zhang, M.; Wang, Q.; Xu, G.; He, H. Ceria-Trapped Single-Atom Rhodium Catalysts for Efficient Ethanol Steam Reforming to Hydrogen. *Catal. Sci. Technol.* **2025**, *15*, 3613–3625. [CrossRef]
45. Grzybek, G.; Ciemierkiewicz, J.; Stelmachowski, P.; Legutko, P.; Adamski, A.; Greluk, M.; Słowik, G.; Kierys, A.; Kotarba, A. Robust Ethanol Steam Reforming Catalysts with Strong Cobalt-Alumina Support Interaction. *Fuel* **2026**, *407*, 137241. [CrossRef]
46. Dave, C.D.; Pant, K.K. Renewable Hydrogen Generation by Steam Reforming of Glycerol over Zirconia Promoted Ceria Supported Catalyst. *Renew. Energy* **2011**, *36*, 3195–3202. [CrossRef]
47. Nichele, V.; Signoretto, M.; Menegazzo, F.; Gallo, A.; Dal Santo, V.; Cruciani, G.; Cerrato, G. Glycerol Steam Reforming for Hydrogen Production: Design of Ni Supported Catalysts. *Appl. Catal. B Environ.* **2012**, *111–112*, 225–232. [CrossRef]
48. Charisiou, N.D.; Papageridis, K.N.; Tzounis, L.; Sebastian, V.; Hinder, S.J.; Baker, M.A.; AlKetbi, M.; Polychronopoulou, K.; Goula, M.A. Ni Supported on CaO-MgO-Al_2O_3 as a Highly Selective and Stable Catalyst for H_2 Production via the Glycerol Steam Reforming Reaction. *Int. J. Hydrogen Energy* **2019**, *44*, 256–273. [CrossRef]
49. Charisiou, N.D.; Siakavelas, G.; Tzounis, L.; Dou, B.; Sebastian, V.; Hinder, S.J.; Baker, M.A.; Polychronopoulou, K.; Goula, M.A. Ni/Y_2O_3–ZrO_2 Catalyst for Hydrogen Production through the Glycerol Steam Reforming Reaction. *Int. J. Hydrogen Energy* **2020**, *45*, 10442–10460. [CrossRef]
50. Veiga, S.; Bussi, J. Steam Reforming of Crude Glycerol over Nickel Supported on Activated Carbon. *Energy Convers. Manag.* **2017**, *141*, 79–84. [CrossRef]
51. Surendar, M.; Sagar, T.V.; Babu, B.H.; Lingaiah, N.; Rao, K.S.R.; Prasad, P.S.S. Glycerol Steam Reforming over La–Ce–Co Mixed Oxide-Derived Cobalt Catalysts. *RSC Adv.* **2015**, *5*, 45184–45193. [CrossRef]
52. Charisiou, N.D.; Italiano, C.; Pino, L.; Sebastian, V.; Vita, A.; Goula, M.A. Hydrogen Production via Steam Reforming of Glycerol over Rh/γ-Al_2O_3 Catalysts Modified with CeO_2, MgO or La_2O_3. *Renew. Energy* **2020**, *162*, 908–925. [CrossRef]
53. Macedo, M.S.; Kraleva, E.; Ehrich, H.; Soria, M.A.; Madeira, L.M. Ni-Based Catalysts Supported on La/AlZn/AlLa Oxides for Hydrogen Production via Glycerol Steam Reforming. *Renew. Energy* **2024**, *223*, 120076. [CrossRef]
54. Wang, Y.; Chen, Y.; Zhu, S.; Song, D.; Ai, T.; He, S.; Luo, Y. Ni/CeO_2 Catalysts for Glycerol Steam Reforming: Effect of Calcination Modes on the Catalytic Performance. *Int. J. Hydrogen Energy* **2024**, *65*, 804–816. [CrossRef]
55. Reynoso, A.J.; Iriarte-Velasco, U.; Gutiérrez-Ortiz, M.A.; Ayastuy, J.L. Cobalt Aluminate Spinel-Derived Catalysts for Glycerol Steam Reforming. *J. Ind. Eng. Chem.* **2024**, *132*, 111–122. [CrossRef]
56. Luisetto, I.; Charisiou, N.D.; Tsiotsias, A.I.; Latsiou, A.I.; Siakavelas, G.; Sebastian, V.; Zhang, R.; Di Bartolomeo, E.; Polychronopoulou, K.; Goula, M.A. Enhanced Glycerol Steam Reforming Using Ni-Doped $CaZrO_3$, $SrZrO_3$, and $BaZrO_3$ Perovskite Oxides. *Int. J. Hydrogen Energy* **2025**, *128*, 574–588. [CrossRef]
57. Wang, Y.; Yu, Y.; Liang, D.; Li, C.; Xin, H.; Wang, J.; Chen, M. Glycerol Steam Reforming for Hydrogen over Mo-Modified Attapulgite-Based Zeolite-Supported Ni-Based Catalysts. *ACS Sustain. Chem. Eng.* **2026**, *14*, 8996–9012. [CrossRef]
58. Argyle, M.; Bartholomew, C. Heterogeneous Catalyst Deactivation and Regeneration: A Review. *Catalysts* **2015**, *5*, 145–269. [CrossRef]
59. Bartholomew, C.H. Mechanisms of Catalyst Deactivation. *Appl. Catal. A Gen.* **2001**, *212*, 17–60. [CrossRef]
60. Sehested, J. Four Challenges for Nickel Steam-Reforming Catalysts. *Catal. Today* **2006**, *111*, 103–110. [CrossRef]
61. Bañares, M.A. Operando Methodology: Combination of in Situ Spectroscopy and Simultaneous Activity Measurements under Catalytic Reaction Conditions. *Catal. Today* **2005**, *100*, 71–77. [CrossRef]
62. Azenha, C.; Lagarteira, T.; Mateos-Pedrero, C.; Mendes, A. Production of Hydrogen from Methanol Steam Reforming Using CuPd/ZrO_2 Catalysts—Influence of the Catalytic Surface on Methanol Conversion and CO Selectivity. *Int. J. Hydrogen Energy* **2021**, *46*, 17490–17499. [CrossRef]
63. Jones, S.D.; Hagelin-Weaver, H.E. Steam Reforming of Methanol over CeO_2- and ZrO_2-Promoted Cu-ZnO Catalysts Supported on Nanoparticle Al_2O_3. *Appl. Catal. B Environ.* **2009**, *90*, 195–204. [CrossRef]
64. Agrell, J.; Birgersson, H.; Boutonnet, M. Steam Reforming of Methanol over a Cu/ZnO/Al_2O_3 Catalyst: A Kinetic Analysis and Strategies for Suppression of CO Formation. *J. Power Sources* **2002**, *106*, 249–257. [CrossRef]
65. Navarro, R.M.; Melián-Cabrera, I.; Boutonnet, M.; Birgersson, H.; Agrell, J.; Fierro, J.L.G. Production of Hydrogen from Methanol over Cu/ZnO Catalysts Promoted by ZrO_2 and Al_2O_3. *J. Catal.* **2003**, *219*, 389–403. [CrossRef]

66. Purnama, H.; Ressler, T.; Jentoft, R.E.; Soerijanto, H.; Schlögl, R.; Schomäcker, R. CO Formation/Selectivity for Steam Reforming of Methanol with a Commercial $CuO/ZnO/Al_2O_3$ Catalyst. *Appl. Catal. A Gen.* **2004**, *259*, 83–94. [CrossRef]
67. Iwasa, N.; Masuda, S.; Takezawa, N. Steam Reforming of Methanol over Ni, Co, Pd and Pt Supported on ZnO. *React. Kinet. Catal. Lett.* **1995**, *55*, 349–353. [CrossRef]
68. Chin, Y.-H.; Dagle, R.A.; Hu, J.; Dohnalkova, A.C.; Wang, Y. Steam Reforming of Methanol over Highly Active Pd/ZnO Catalyst. *Catal. Today* **2002**, *77*, 79–88. [CrossRef]
69. Köwitsch, N.; Thoni, L.; Klemmed, B.; Benad, A.; Paciok, P.; Heggen, M.; Eychmüller, A.; Armbrüster, M. Unprecedented Catalytic Activity and Selectivity in Methanol Steam Reforming by Reactive Transformation of Intermetallic In–Pt Compounds. *J. Phys. Chem. C* **2021**, *125*, 9809–9817. [CrossRef]
70. Fornari, A.C.; Pimenta, J.L.C.W.; Dos Santos, O.A.A.; De Matos Jorge, L.M. Statistical Optimization of the Composition of $CuO–ZnO/Al_2O_3$ Catalysts for Methanol Steam Reforming. *Braz. J. Chem. Eng.* **2021**, *38*, 523–548. [CrossRef]
71. Llorca, J.; Homs, N.; Sales, J.; De La Piscina, P.R. Efficient Production of Hydrogen over Supported Cobalt Catalysts from Ethanol Steam Reforming. *J. Catal.* **2002**, *209*, 306–317. [CrossRef]
72. Llorca, J.; Homs, N.; Ramirez De La Piscina, P. In Situ DRIFT-Mass Spectrometry Study of the Ethanol Steam-Reforming Reaction over Carbonyl-Derived Co/ZnO Catalysts. *J. Catal.* **2004**, *227*, 556–560. [CrossRef]
73. Haga, F.; Nakajima, T.; Yamashita, K.; Mishima, S. Effect of Crystallite Size on the Catalysis of Alumina-Supported Cobalt Catalyst for Steam Reforming of Ethanol. *React. Kinet. Catal. Lett.* **1998**, *63*, 253–259. [CrossRef]
74. Kaddouri, A.; Mazzocchia, C. A Study of the Influence of the Synthesis Conditions upon the Catalytic Properties of Co/SiO_2 or Co/Al_2O_3 Catalysts Used for Ethanol Steam Reforming. *Catal. Commun.* **2004**, *5*, 339–345. [CrossRef]
75. Fatsikostas, A.N.; Verykios, X.E. Reaction Network of Steam Reforming of Ethanol over Ni-Based Catalysts. *J. Catal.* **2004**, *225*, 439–452. [CrossRef]
76. Song, H.; Zhang, L.; Watson, R.; Braden, D.; Ozkan, U. Investigation of Bio-Ethanol Steam Reforming over Cobalt-Based Catalysts. *Catal. Today* **2007**, *129*, 346–354. [CrossRef]
77. Batista, M.S.; Santos, R.K.S.; Assaf, E.M.; Assaf, J.M.; Ticianelli, E.A. Characterization of the Activity and Stability of Supported Cobalt Catalysts for the Steam Reforming of Ethanol. *J. Power Sources* **2003**, *124*, 99–103. [CrossRef]
78. Breen, J.P.; Burch, R.; Coleman, H.M. Metal-Catalysed Steam Reforming of Ethanol in the Production of Hydrogen for Fuel Cell Applications. *Appl. Catal. B Environ.* **2002**, *39*, 65–74. [CrossRef]
79. Vaidya, P.D.; Rodrigues, A.E. Insight into Steam Reforming of Ethanol to Produce Hydrogen for Fuel Cells. *Chem. Eng. J.* **2006**, *117*, 39–49. [CrossRef]
80. Sun, J.; Qiu, X.; Wu, F.; Zhu, W.; Wang, W.; Hao, S. Hydrogen from Steam Reforming of Ethanol in Low and Middle Temperature Range for Fuel Cell Application. *Int. J. Hydrogen Energy* **2004**, *29*, 1075–1081. [CrossRef]
81. Srinivas, D.; Satyanarayana, C.V.V.; Potdar, H.S.; Ratnasamy, P. Structural Studies on $NiO-CeO_2-ZrO_2$ Catalysts for Steam Reforming of Ethanol. *Appl. Catal. A Gen.* **2003**, *246*, 323–334. [CrossRef]
82. Xu, W.; Liu, Z.; Johnston-Peck, A.C.; Senanayake, S.D.; Zhou, G.; Stacchiola, D.; Stach, E.A.; Rodriguez, J.A. Steam Reforming of Ethanol on Ni/CeO_2: Reaction Pathway and Interaction between Ni and the CeO_2 Support. *ACS Catal.* **2013**, *3*, 975–984. [CrossRef]
83. Slinn, M.; Kendall, K.; Mallon, C.; Andrews, J. Steam Reforming of Biodiesel By-Product to Make Renewable Hydrogen. *Bioresour. Technol.* **2008**, *99*, 5851–5858. [CrossRef] [PubMed]
84. Hirai, T.; Ikenaga, N.; Miyake, T.; Suzuki, T. Production of Hydrogen by Steam Reforming of Glycerin on Ruthenium Catalyst. *Energy Fuels* **2005**, *19*, 1761–1762. [CrossRef]
85. Adhikari, S.; Fernando, S.D.; To, S.D.F.; Bricka, R.M.; Steele, P.H.; Haryanto, A. Conversion of Glycerol to Hydrogen via a Steam Reforming Process over Nickel Catalysts. *Energy Fuels* **2008**, *22*, 1220–1226. [CrossRef]
86. Douette, A.M.D.; Turn, S.Q.; Wang, W.; Keffer, V.I. Experimental Investigation of Hydrogen Production from Glycerin Reforming. *Energy Fuels* **2007**, *21*, 3499–3504. [CrossRef]
87. Pompeo, F.; Santori, G.; Nichio, N.N. Hydrogen and/or Syngas from Steam Reforming of Glycerol. Study of Platinum Catalysts. *Int. J. Hydrogen Energy* **2010**, *35*, 8912–8920. [CrossRef]
88. Adhikari, S.; Fernando, S.D.; Haryanto, A. Hydrogen Production from Glycerin by Steam Reforming over Nickel Catalysts. *Renew. Energy* **2008**, *33*, 1097–1100. [CrossRef]
89. Iriondo, A.; Barrio, V.L.; Cambra, J.F.; Arias, P.L.; Güemez, M.B.; Navarro, R.M.; Sanchez-Sanchez, M.C.; Fierro, J.L.G. Influence of La_2O_3 Modified Support and Ni and Pt Active Phases on Glycerol Steam Reforming to Produce Hydrogen. *Catal. Commun.* **2009**, *10*, 1275–1278. [CrossRef]
90. Cui, Y.; Galvita, V.; Rihko-Struckmann, L.; Lorenz, H.; Sundmacher, K. Steam Reforming of Glycerol: The Experimental Activity of $La_{1-x}Ce_xNiO_3$ Catalyst in Comparison to the Thermodynamic Reaction Equilibrium. *Appl. Catal. B Environ.* **2009**, *90*, 29–37. [CrossRef]

91. Zhang, B.; Tang, X.; Li, Y.; Xu, Y.; Shen, W. Hydrogen Production from Steam Reforming of Ethanol and Glycerol over Ceria-Supported Metal Catalysts. *Int. J. Hydrogen Energy* **2007**, *32*, 2367–2373. [CrossRef]
92. Dou, B.; Dupont, V.; Rickett, G.; Blakeman, N.; Williams, P.T.; Chen, H.; Ding, Y.; Ghadiri, M. Hydrogen Production by Sorption-Enhanced Steam Reforming of Glycerol. *Bioresour. Technol.* **2009**, *100*, 3540–3547. [CrossRef] [PubMed]
93. Choi, Y.; Kim, N.D.; Baek, J.; Kim, W.; Lee, H.J.; Yi, J. Effect of N_2O-Mediated Calcination on Nickel Species and the Catalytic Activity of Nickel Catalysts Supported on γ-Al_2O_3 in the Steam Reforming of Glycerol. *Int. J. Hydrogen Energy* **2011**, *36*, 3844–3852. [CrossRef]
94. Shejale, A.D.; Yadav, G.D. Ni–Cu and Ni–Co Supported on La–Mg Based Metal Oxides Prepared by Coprecipitation and Impregnation for Superior Hydrogen Production via Steam Reforming of Glycerol. *Ind. Eng. Chem. Res.* **2018**, *57*, 4785–4797. [CrossRef]
95. Buffoni, I.N.; Gatti, M.N.; Santori, G.F.; Pompeo, F.; Nichio, N.N. Hydrogen from Glycerol Steam Reforming with a Platinum Catalyst Supported on a SiO_2 -C Composite. *Int. J. Hydrogen Energy* **2017**, *42*, 12967–12977. [CrossRef]
96. Cheng, Z.; Li, Y.; Wang, M.; He, L.; Zhang, L.; Jin, Y.F.; Lan, G.; Sun, X.; Qiu, Y.; Li, Y. Construction of Porous Cu/CeO_2 Catalyst with Abundant Interfacial Sites for Effective Methanol Steam Reforming. *J. Colloid Interface Sci.* **2025**, *677*, 55–67. [CrossRef] [PubMed]
97. Hu, Y.; He, W.; Shen, Y. Hydrogen Production from Ethanol by Steam Reforming with Recyclable $NiCaO_x$/NaCl Catalysts. *Catal. Sci. Technol.* **2024**, *14*, 1062–1071. [CrossRef]
98. Iglesias-Vázquez, S.; Valecillos, J.; Remiro, A.; Valle, B.; Bilbao, J.; Gayubo, A.G. Global Vision of the Reaction and Deactivation Routes in the Ethanol Steam Reforming on a Catalyst Derived from a Ni–Al Spinel. *Energy Fuels* **2024**, *38*, 7033–7048. [CrossRef] [PubMed]
99. Liao, M.; Qin, C.; Xu, L.; Guo, S.; Wang, C.; Li, Y.; Liu, W.; Song, Q.; Chen, Y.; Du, Y. Quinary Metal Oxide $NiCoMnCeCaO_x$ Nanorod as a Multifunctional Catalyst towards Hydrogen Production from Ethanol Steam Reforming: Synergistic Effect of Polymetallic Component. *Chem. Eng. J.* **2024**, *497*, 154646. [CrossRef]
100. Zhang, H.; Millan, M.G.; Chen, Z.; Li, T.; Cui, Z.; Yuan, G. Steam Reforming of Glycerol for Co-Producing Hydrogen and Carbon Nanotubes over Nanoscale Ni-Based Catalysts: Insights into Support Effect and Carbon Deposition. *Int. J. Hydrogen Energy* **2025**, *105*, 896–909. [CrossRef]

Disclaimer/Publisher's Note: The statements, opinions and data contained in all publications are solely those of the individual author(s) and contributor(s) and not of MDPI and/or the editor(s). MDPI and/or the editor(s) disclaim responsibility for any injury to people or property resulting from any ideas, methods, instructions or products referred to in the content.